Energy Advances

Accepted Manuscript

This article can be cited before page numbers have been issued, to do this please use: V. Aravindan and A. Viswanathan, *Energy Adv.*, 2025, DOI: 10.1039/D4YA00617H.

ROYAL SOCIETY OF CHEMISTRY

rsc.li/energy-advances

View Article Online
DOI: 10.1039/D4YA00617H

Durable, Rate Capable and High Energy Hybrid Supercapacitor From PANI/ZnO/SnO_2 Nanocomposite with Zero-Waste Electrolyte Approach

Aranganathan Viswanathan, and Vanchiappan Aravindan**

Department of Chemistry, Indian Institute of Science Education and Research (IISER), Tirupati-517619, Andhra Pradesh, India.

ABSTRACT

A hybrid supercapacitor material, polyaniline/ZnO/SnO_2 of weight percentages of 58.34%: 8.33%:33.33% (PZnSn), respectively, was synthesized in a facile *in-situ* single-step method. Remarkably, the constituent ZnO was synthesized at 90 ˚C in an in-situ single-step method along with two other constituents in 2 hrs. The astonishment is due to the point that the synthesis of ZnO generally involves calcination at high temperatures for a longer duration. The energy storage performance was evaluated with two aqueous electrolytes, viz., 1 M H_2SO_4 (SA) and the liquid by-product that was obtained after the synthesis of PANI (SLP). The SLP provided 57.25% higher energy storage performance in relation to that provided by the SA. The PZnSn exhibited a durable and rate-capable energy storage property by exhibiting robustness up to 16,500 cycles at 0.4 V s^{-1} and 39 A g^{-1}, respectively, in the presence (ITP) of SA and up to 15,000 cycles at 0.4 V s^{-1} and 42 A g^{-1} ITP of SLP, respectively, in a real-time symmetric two electrode systems. The PZnSn displayed a remarkable trait of enhancement of energy storage with an increase in the number of charge and discharge cycles ITP of both the electrolytes. However, the enhancement provided by

View Article Online
DOI: 10.1039/D4YA00617H

SLP is higher than that of SA. The maximum performance achieved from PZnSn ITP of SLP is a Q of 347.2 C g^{-1}, an E of 57.87 W h kg^{-1} (comparable with Ni-Cd batteries) and a P of 1.2 kW kg^{-1} at 1 A g^{-1}.

KEYWORDS: Hybrid supercapacitor, Stannic oxide, Zinc oxide, green electrolyte, by-product of PANI.

Email IDs: ranguchemist@gmail.com (AV), and aravind.van@gmail.com (VA)

INTRODUCTION

Hybrid supercapacitors are devices that contain electrode material that exhibits energy storage characteristics of both capacitive and battery types. Such materials are believed to impart high energy characteristics closer to batteries in terms of their specific energy (E), with the high specific power (P) of capacitors and supercapacitors. The combination of characters of both batteries and capacitors could be made by integrating both capacitive or pseudocapacitive type electrode materials with battery-type materials. The capacitive-type material involves surface capacitive processes (electrical double-layer formation and fast redox reactions) in energy storage, and the battery-type material involves bulk processes like intercalation. The combination of both surface and bulk energy storage processes is essential for achieving the high energy character in a charge storage device.

The well-known pseudocapacitive material and a conducting polymer is polyaniline (PANI)[1,2], which is involved in the pseudocapacitive process by its redox transformation between the leucoemaraldine, emaraldine and pernigraniline forms[3]. In addition, it is expensive, facile to

View Article Online
DOI: 10.1039/D4YA00617H

synthesize, environmentally friendly, non-toxic, and has a theoretical specific capacity (Q) of ~294 mAh g^{-1}[4,5]. The SnO_2 is a known battery-type material[6–8] (theoretical Q of ~790 mAh g^{-1}[9]), easy to synthesize, and involves the bulk process of energy storage predominantly. The ZnO is used in both batteries[10–13] and supercapacitors[14–19] for its versatile nature of both pseudocapacitive and battery-type energy storage behavior. The synthesis of ZnO in the wet method at low temperatures is not common, but it can be synthesized in the chemical reduction method not as an individual entity but with other metal derivatives when the purpose of the synthesis is to produce a double metal oxide, as reported in our earlier study [5]. The electrolytes used in the supercapacitors are as imperative as other elements, as they play an essential role in determining the potential window and the quantity of energy stored in energy storage devices. The use of liquid by-products obtained after the synthesis of PANI was studied to be an effective method to increase the energy storage and the rate capability of the supercapacitors[20,21]. The use of this liquid by-product of the synthesis of PANI has exhibited 40 % [21] and 22 % [20] enhancement in energy storage in PANI-containing supercapacitors in relation to the conventional 1 M H_2SO_4. Therfore, it is intended to further explore the capability of this liquid by-product of the synthesis of PANI in this study.

Herein, an attempt has been made to produce a hybrid supercapacitor electrode material by integrating PANI, ZnO and SnO_2 (PZnSn) by facile *in-situ* single-step method ITP of two electrolytes, which are 1 M H_2SO_4 and the liquid by-product of the synthesis of PANI. As this combination can undergo EDL formation, pseudocapactive reactions with a higher number of electrons are involved, and the bulk process of H^+ intercalation is performed. It is anticipated that PZnSn will exhibit high-energy hybrid supercapacitor behavior. The synthetic method structural and energy storage characterizations of PZnSn are provided in the following sections.

EXPERIMENTAL SECTION

View Article Online
DOI: 10.1039/D4YA00617H

Synthesis of polyaniline, zinc oxide and stannic oxide (PANI/ZnO/SnO_2) (PZnSn) nanocomposite

The synthesis of the PZnSn composite was conducted based on the synthetic procedure mentioned in in the granted Indian patent [22]. In the synthesis of PZnSn, the 350 µL of aniline was mixed with 100 mL distilled water (DW) and stirred for 15 minutes, then 1.4 g of ammonium persulfate dissolved in a minimum amount of DW was added, following which 10 mL of 2 M CH_3SO_3H was also added as dopant and the reaction content was stirred at room temperature for 5 hrs. After 5 hrs of oxidative polymerization, the pH of the reaction mixture was raised to 14 using 6 M NaOH and then the reduction reaction of the content was carried out using an appropriate amount of hydrazine hydrate for 2 hrs at 90°C. After 2 hrs of reduction reaction, 13.27 mL of $SnCl_4.5\ H_2O$ and 5 mL of $ZnSO_4.7\ H_2O$ were mixed and stirred at 45°C for 30 minutes. Then, the reaction mixture was cooled, and the targeted composite of PZnSn was extracted from the reaction mixture using the method mentioned in [20]. Thus, the PANI/ZnO/SnO_2 composite was obtained, and the weight composition of the composite was PANI 58.34%:ZnO 8.33%:SnO_2 33.33%. The synthesis of PANI and its by-products are provided in the supporting information (section S1). The characterization (S2) and fabrication (S3) details are provided in the supporting information.

Uniqueness of the synthetic method

The synthesis of PANI/ZnO/SnO_2 is unique as it provides the composite containing ZnO at a lower temperature of 80 °C in 2 h without using any sophisticated setups and apparatuses because generally the synthesis of ZnO involves the synthesis of $Zn(OH)_2$ by treating the solutions of zinc salt with bases like NaOH or KOH, and then calcinating the $Zn(OH)_2$ at 500 °C for getting the ZnO[23]. ZnO is also synthesized using the hydrothermal method by heating the $Zn(OH)_2$ at 150 - 200 °C in an autoclave [24–26]. The sol-gel method involves heating the sol-gel at 150 °C for 5 h[27]; the microemulsion method involves heating the emulsion at 140 °C for 5 h with reflux condenser[28].

View Article Online
DOI: 10.1039/D4YA00617H

The solvothermal method involves heating at 120 °C for 5 h in a teflon-lined stainless steel autoclave[29]; the electrochemical deposition involves a three-electrode cell setup with the electrolyte of a mixture of $Zn(NO_3)_2$, KNO_3 and KCl at 80 °C[30], one of the wet chemical methods involve the heating of a mixture of aqueous solution $Zn(NO_3)_2$ and ammonia at 120 °C with reflux condenser for 12 h[31], the flux method involves the reagents of ZnO at temperatures of range 450 to 900 °C for 1 to 120 h [32], the electrospinning method involves the mixture of PVA and zinc acetate, a high voltage of 20 kV, and high-temperature calcination of 500 °C for 4-10 h[33], the microwave method involves the exposure of reagents of ZnO to microwave produced at 510 to 680 W for 10 to 15 min[34] and the polyol method involves the heating the reagents of ZnO at 180 °C for 30 min[35]. Other than these solution-based methods, vapor phase approaches are also available for synthesizing ZnO and which are molecular beam epitaxy (MBE), thermal evaporation, physical vapor deposition, plasma enhanced chemical vapor deposition (PECVD), chemical vapor deposition, metal-organic chemical vapor deposition (MOCVD), and pulsed laser deposition[36]. These methods are also not free from sophisticated setups and apparatuses. In addition, the synthesis of composites of ZnO with PANI generally involves two-step synthesis, that is, synthesizing the PANI or PANI-containing composite and then adding pre-synthesized ZnO or adding the ZnO to PANI during its oxidative polymerization[37–42] but here in this synthesis method the composite of ZnO made in the single step. Therefore, the presented method of synthesis of ZnO composite is facile, unique, scalable and effective.

The usage of the liquid by-product that is attained after the synthesis of PANI as an electrolyte for supercapacitors is unique and beneficial, as proved in our early studies of [5,20,21]. The usage of the liquid by-product of PANI and a liquid by-product of electrode composite after acidification has enhanced energy storage and aided the supercapacitors in moving to the realms

View Article Online
DOI: 10.1039/D4YA00617H

of batteries in terms of their specific energies. This approach of waste to wealth approach not only enhances the energy storage to significant extent but also reduces the waste discharged into the environment and reduces the cost involved in the domain of energy storage and conversion.

RESULTS AND DISCUSSION

Structural characterizations

The XRD pattern of PZnSn (Figure. 1a) contains peaks corresponding to (002), (101), (200), (112) and (201) planes of ZnO (JCPDS No.: 01-1136) at 34.35°, 36.20°, 66.38°, 67.92° and 68.95°, respectively (Figure. S1). The peak corresponding to the plane of (211) of SnO_2 is seen at 51.74 (JCPDS No.: 41-1445).

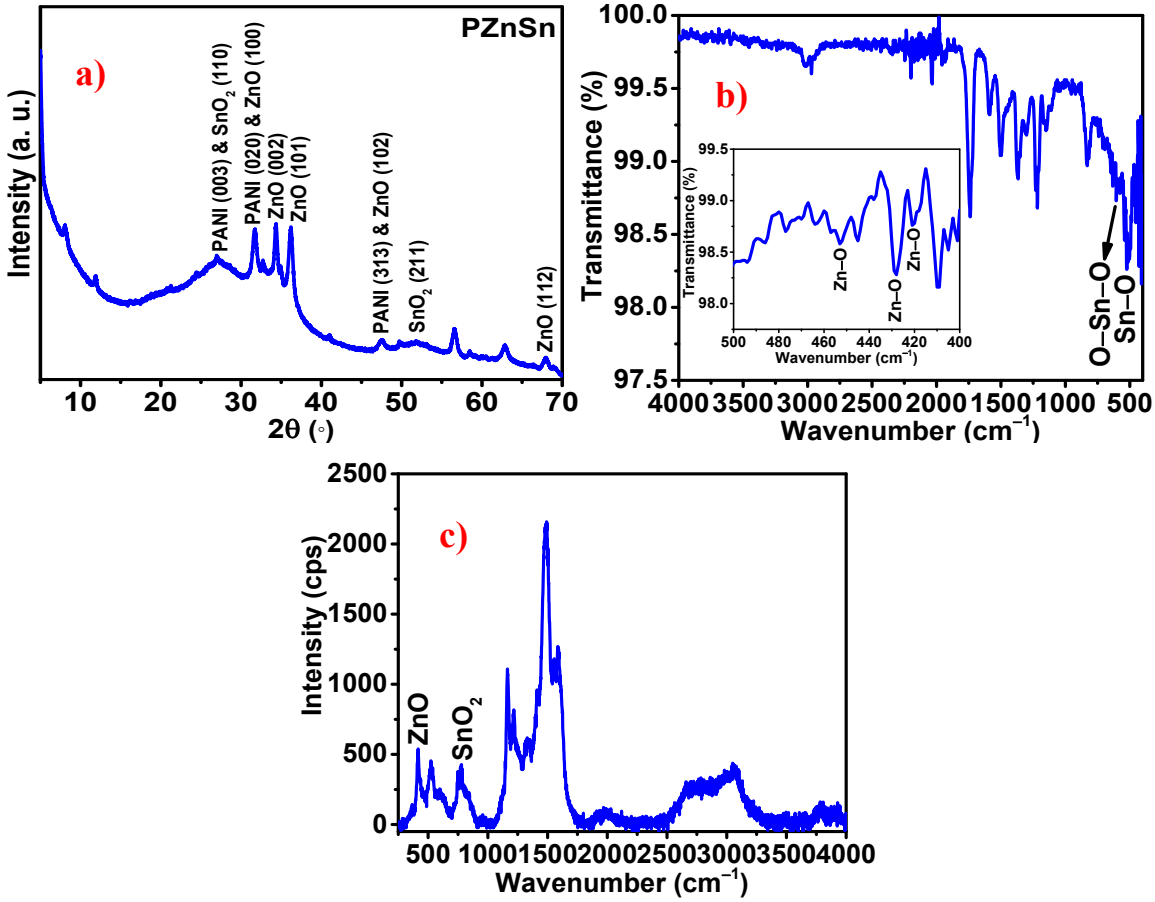

View Article Online
DOI: 10.1039/D4YA00617H

Figure 1. a) XRD pattern, b) FT-IR, and c) Raman spectrum of PZnSn.

The peak at 26.95° is brought by both (110) plane of SnO_2 and (003) plane of PANI (JCPDS No.: 53-1717) (Figure. S2). The peak at 31.69° corresponds to both (100) plane of ZnO and (020) plane of PANI. The peak at 47.50° corresponds to both (102) plane of ZnO and (313) plane of PANI (Figure. S3). Thus, the characteristic peaks of constituents confirm the successful synthesis of the PZnSn composite. The FT-IR peak positions and the corresponding species are presented in supporting information (section S3). The Raman peaks (Figure. 1c) at 415(E_1)[43] and 778 cm^{-1} (B_{2g})[44] are corresponding to ZnO and SnO_2, respectively. The peaks at 1163, 1217, and 1491 cm^{-1} are due to C–H of benzenoid rings, C–N stretching of poloranic segments[44] and C=N stretching vibrations of quinoid rings[45] of PANI, respectively. The peaks at 1332, 1412, 1556 and 1586 cm^{-1} are also due to different vibrations of PANI[44].

The FE-SEM images (Figure.2) depict the morphology of PZnSn, in which the PANI is seen to be in the fiber morphology and the nanoparticles of ZnO and SnO_2 are dispersed well across the bulk of the PZnSn. The PZnSn also has pores across its morphology to facilitate the effective electrolytic permeation across the PZnSn nanocomposite. The diameter of PANI nanofibers is 38 to 54 nm, and that of pores is 59 to 88 nm (Figure. S4). The elemental maps (Figure. S5) of PZnSn evidently depict the effective dispersion of the elements and, in turn, the constituents across the PZnSn composite.

View Article Online
DOI: 10.1039/D4YA00617H

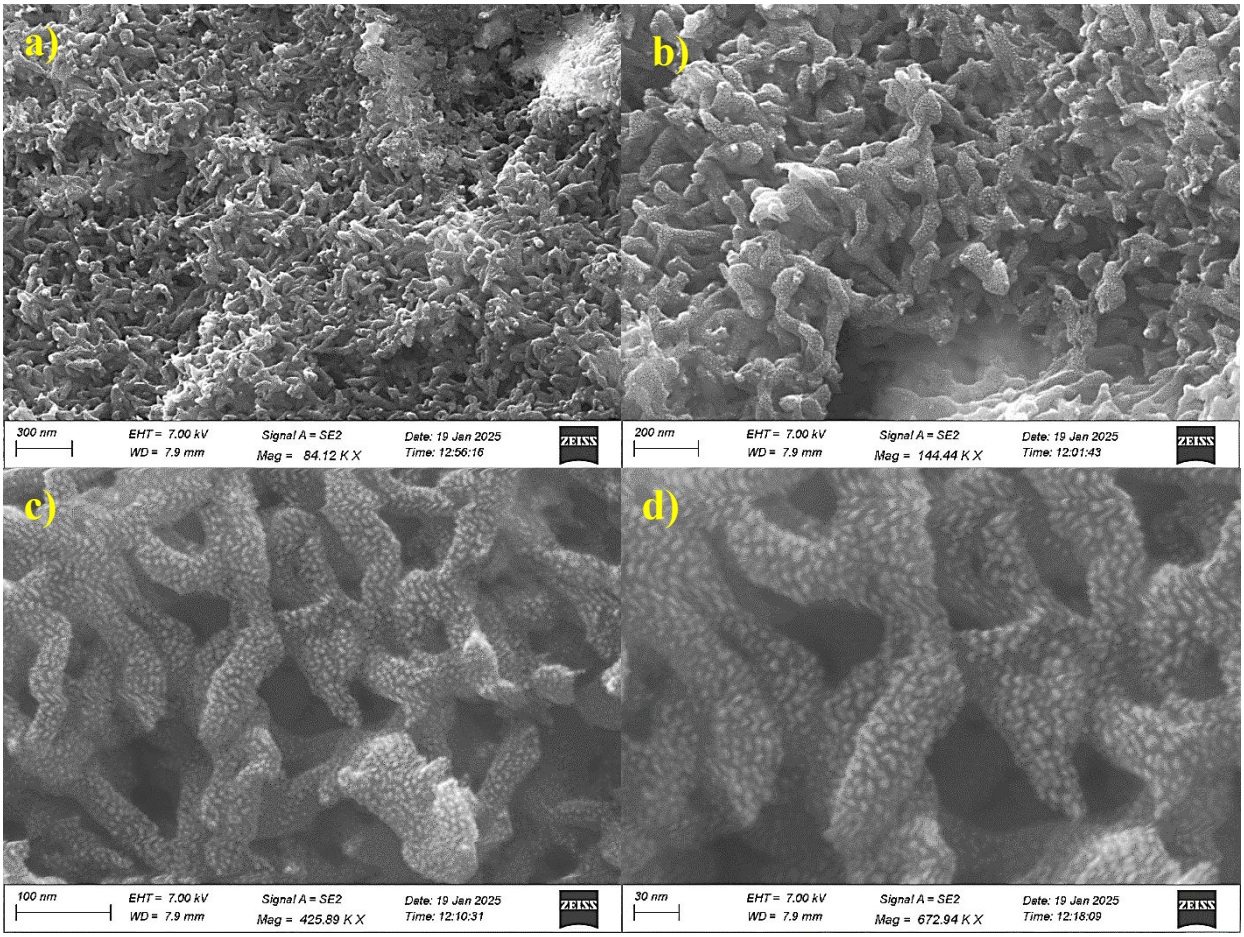

Figure 2. (a-d) FE-SEM images of PZnSn at different magnifications.

View Article Online
DOI: 10.1039/D4YA00617H

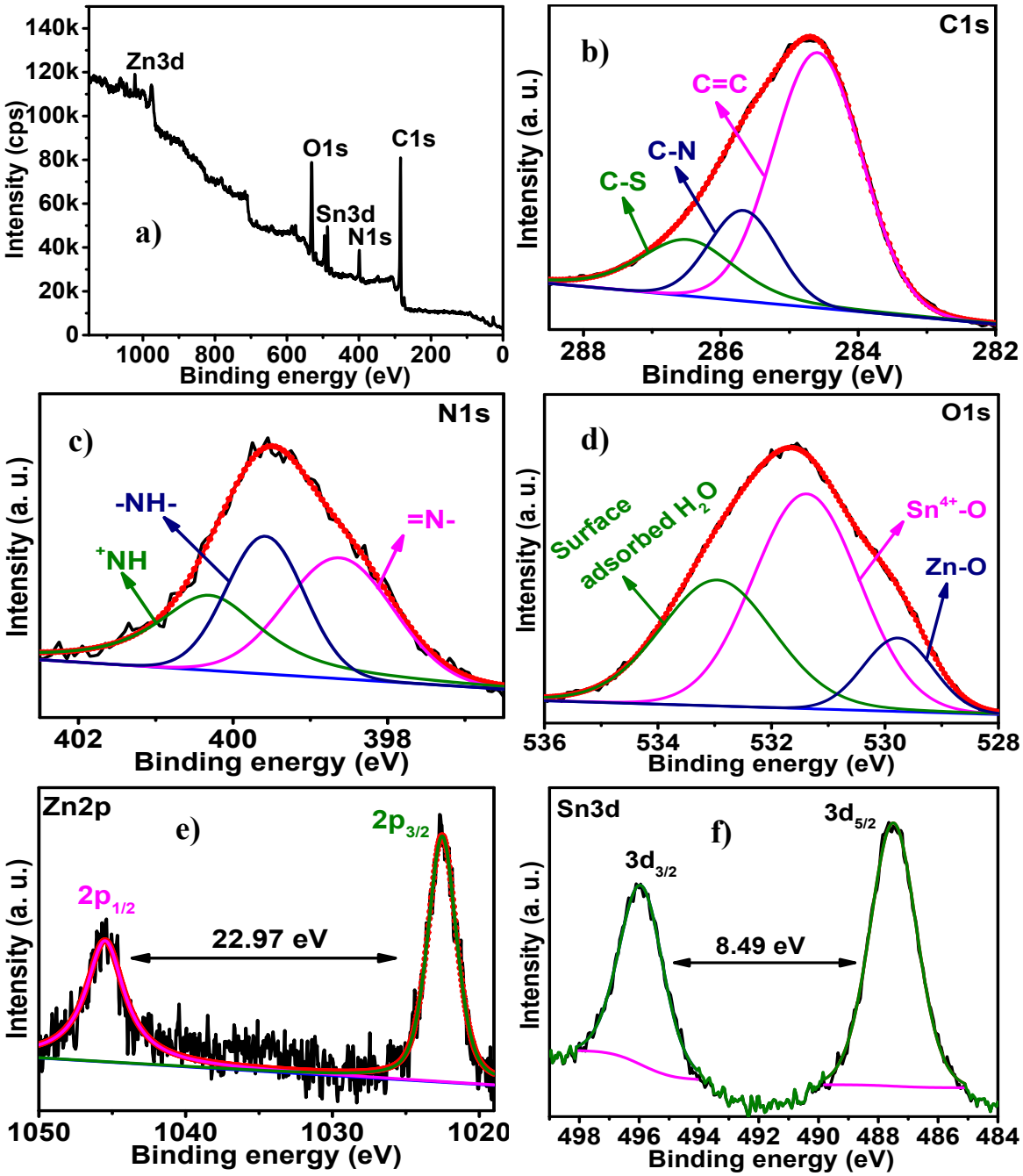

Figure 3. XPS a) survey spectrum, core level spectra of b) C1s, c) N1s, d) O1s, e) Zn2p and f) Sn3d of PZnSn.

The XPS survey spectrum of PZnSn (Figure. 3a) composite contains the characteristic peaks of elements of PZnSn. The chemical nature of the elements was deduced by the deconvolution

View Article Online
DOI: 10.1039/D4YA00617H

process of the core level spectrum of each elements. The obtained peaks in the deconvolution process and their respective chemical nature of the elements confirm that the chemical forms of elements present in PZnSn are PANI, ZnO and SnO_2 (Table 1).

Table 1 XPS peak positions and their respective chemical species

Element	Binding energy (eV) and species
C 1s	284.60 eV (C=C), 285.7 eV (C–N) and 286.53 eV (C–S)[44] (Figure. 3a)
N 1s	398.63 eV (=N–), 399.58 eV (–NH–) and 400.32 eV ($^{+}$NH)[3] (Figure. 3b)
O 1s	529.79 eV (Zn–O)[46,47], 531.39 eV (Sn^{4+}–O)[44] and 532.98 eV (surface absorbed H_2O)[44] (Figure. 3c)
Zn 2p	1022.53 eV ($2p_{3/2}$)[48] and 1045.5 eV ($2p_{1/2}$) (doublet energy difference – 22.97 eV) [49] (Figure. 3d)
Sn 3d	487.49 eV ($3d_{5/2}$)[50] and 495.98 eV ($3d_{3/2}$)[51] (doublet energy difference – 8.49 eV)[52] (Figure. 3e)

Electrochemical characterizations

The energy storage performance of the PZnSn composite was assessed in a 2-electrode (2-EL) system using 1 M H_2SO_4 (SA) and liquid by-product obtained after the synthesis of PANI (SLP) as electrolytes. The energy storage study of the PZnSn composite revealed that the PZnSn exhibits promising energy storage characteristics and exhibits a remarkable trait of increased energy storage with an increase in number of cycles ("increase in number of cycles" is abbreviated as INC) during the cyclic stability study at 0.4 V s^{-1} ITP of both the electrolytes. This unique trait is not new, as similar observations have been made in the past with our other materials reported in [3,5,20,53–56]. The energy storage enhancement obtained from ITP of SLP is higher than that ITP of SA. In addition, ITP of SLP's maximum performance of PZnSn was obtained relatively quickly

View Article Online
DOI: 10.1039/D4YA00617H

compared to that ITP of SA. The durability studies were conducted at 0.4 V s^{-1}, up to 16,500 and 15,000 cycles of ITP of SA and SLP, respectively. The maximum performance of PZnSn was brought about after 16,500 and 10,000 cycles of ITP of SA and SLP, respectively. The higher energy storage obtained ITP of SLP suggests the efficient reuse of liquid by-product of PANI as an electrolyte, remarking the point of "waste-to-wealth".

Table 2 The energy storage parameters of PZnSn ITP of SA after DNC at 1 A g^{-1}.

PZnSn	Q (C g^{-1})	E (Wh kg^{-1})	P (kW kg^{-1})	η (%)
Before cyclic study	162.1	27.01	1.2	91.63
After 4000 cycles	169.7	28.28	1.2	84.02
After 10,000 cycles	243.8	40.64	1.2	70.24
After 16,500 cycles	312.0	52.00	1.2	47.81

Table 3 The energy storage parameters of PZnSn ITP of SLP after DNC at 1 A g^{-1}.

PZnSn	Q (C g^{-1})	E (Wh kg^{-1})	P (kW kg^{-1})	η (%)
Before cyclic study	254.9	42.49	1.2	80.08
After 5000 cycles	308.6	51.43	1.2	77.69
After 10,000 cycles	347.2	57.87	1.2	59.85
After 15,000 cycles	288.3	48.06	1.2	68.69

The unique characteristics of the increase in energy storage (Eqn. S1) with INC were characterized at different points of the cyclic stability test, which were before the cyclic study and after 4000, 10,000, and 16,500 cycles for SA and SLP. After "different number of cycles" these points are abbreviated as DNC and used in the following paragraphs. The energy storage

View Article Online
DOI: 10.1039/D4YA00617H

parameters like Q (Eqn. S2), E (Eqn. S3), specific power (P) (Eqn. S4), and columbic efficiency (η) (Eqn. S5) of PZnSn obtained after DNC ITP of SA and SLP are shown in Table 2 and Table 3, respectively.

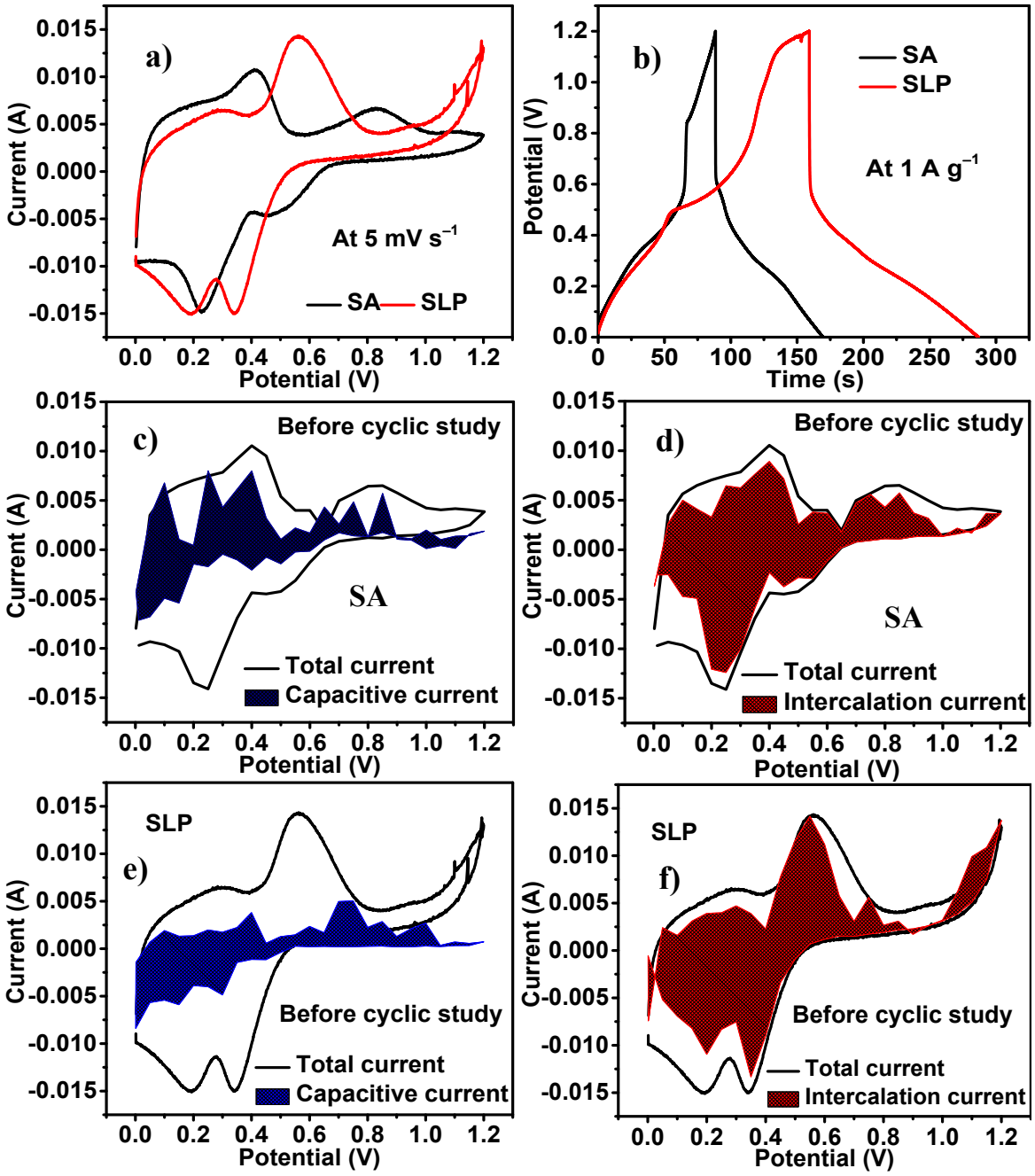

View Article Online
DOI: 10.1039/D4YA00617H

Figure 4. a) CV plots at 5 mV s^{-1}, b) charge and discharge (CD) plots at 1 A g^{-1} of PZnSn ITP of SA and SLP, c) & d) capacitive and intercalation current offered by PZnSn ITP of SA at 5 mV s^{-1}, e) and f) capacitive and intercalation current offered by PZnSn ITP of SLP at 5 mV s^{-1}.

As it is in Table 2, with INC, the Q is increasing, but the η is decreasing ITP of SA. At the end of 16,500 cycles, the obtained η is 47.81%, which is lesser for supercapacitors and therefore, the cyclic stability was paused at this point in the case of SA. In the case of SLP, the energy storage performance begins to deteriorate after 10,000 cycles; therefore, it was stopped after 15,000 cycles. The entire findings and corresponding discussion of PZnSn are as follows.

The higher faradaic area and longer discharge time (t_d) of PZnSn obtained in ITP of SLP are seen in Figure. 4a and Figure.4b, respectively. These higher faradaic areas and t_d indicate the higher energy storage ITP of SLP. The peaks and plateaus of CV plots and charge-discharge (CD) plots of PZnSn indicate its faradaic process of energy storage. As it is seen in the Figure. 4a ITP SLP the PZnSn has exhibited a new faradaic peak, which is attributed to the production of another intercalation process (Fig. 4f) at the potential range of 0.35 to 0.55 V, and which is the merit of usage of SLP and in turn the increased energy brought by it. The Q of PZnSn at 1 A g^{-1} ITP of SA and SLP are 162 and 255 C g^{-1}, respectively. This Q of PZnSn obtained ITP of SLP, which is 57.25% higher than that obtained ITP of SA. This higher Q obtained ITP of SLP is due to the higher occurrence of controlled intercalation reactions in its presence, in relation to that ITP of SA. The percentage contribution surface capacitive processes (EDL + redox reaction) and diffusion-controlled intercalation processes to the energy storage of PZnSn ITP of SA (Figure. 4c and 4d) and SLP (Figure. 4e and 4f) were obtained by the deconvolution of CV curves (Eqn. S6 and Eqn. S7). The percentage of energy stored by capacitive processes and intercalation reactions ITP of SA is 36.36 and 63.64%, respectively, and ITP of SLP are 20.79 and 79.21%, respectively.

View Article Online
DOI: 10.1039/D4YA00617H

This higher percentage of intercalation reactions occurring in ITP of SLP is bringing higher *Q* in PZnSn in its presence.

The sustainability of PZnSn to the higher potential and current loadings is studied by subjecting it to different potential scans and current densities. The PZnSn ITP of both SA and SLP sustains the high potential scan of 0.2 V s^{-1} (Figure. S6a and Figure. 5a). In the case of CD study, the PZnSn sustains up to a current density of 14 and 32 A g^{-1} ITP of SA and SLP, respectively (Figure. S6b, Figure.5b and Figure. 5c).

View Article Online
DOI: 10.1039/D4YA00617H

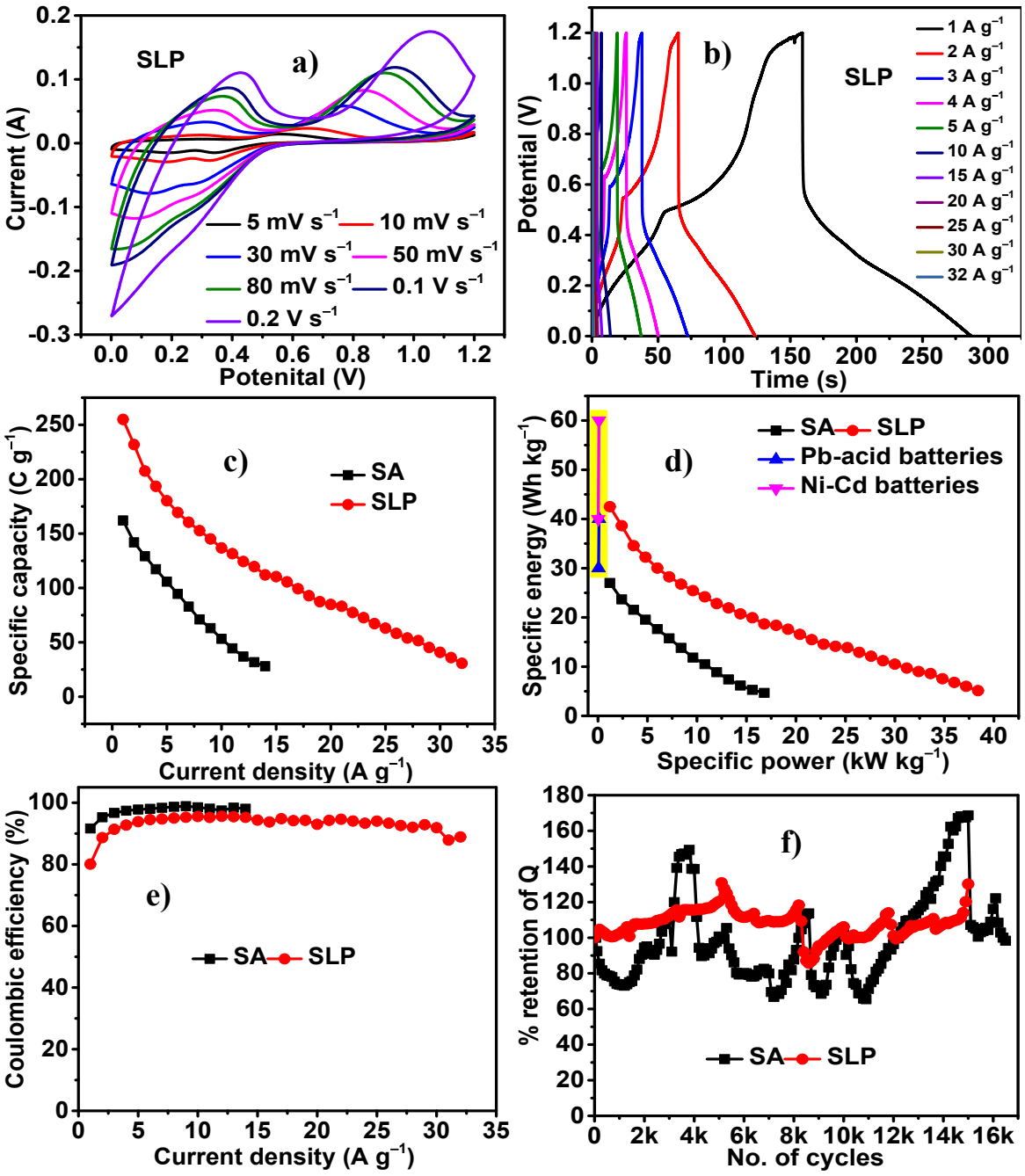

Figure 5. a) CV curves at different scan rates and b) CD curves at different current densities of PZnSn ITP of SLP, c) Plots of specific capacity *vs.* current density, d) plots of specific energy vs specific power, e) plots coulombic efficiency vs current density, and f) % retention of *Q vs.* number of cycles.

View Article Online
DOI: 10.1039/D4YA00617H

The high current sustainability of PZnSn ITP of SLP indicates the better reversibility of energy storage reactions and the least structural degradation that are taking place at higher current loadings in its presence. The Q obtained at 1 and 14 A g^{-1} ITP of SA are 162 and 28 C g^{-1} (17.28% retention), respectively (Figure. 5c).

The Q obtained at 1, 14 and 32 A g^{-1} ITP of SLP are 255, 112 (43.93% retention) and 31 C g^{-1} (12.05% retention), respectively (Figure. 5c). The high rate capability of PZnSn ITP of SLP indicates the better electrolytic diffusion and a similar amount of energy storage reactions even at higher current loadings as they are at lower current loadings. The plots of P *vs*. E (Figure. 5d) of PZnSn are also following a similar trend as that of Figure. 5c. The E and P that are obtained at 1 A g^{-1} are 27.01 Wh kg^{-1} and 1.2 kW kg^{-1}; and 42.49 Wh kg^{-1} and 1.2 Wh kg^{-1} ITP of SA and SLP, respectively. The higher E obtained ITP of SLP is in the same order as those of Pb-lead acid and Ni-Cd batteries[57] (Figure. 5d). The presence of SA provides the higher η at all current densities in PZnSn in comparison with that obtained ITP of SLP. The low η of PZnSn ITP of SLP is due to the higher occurrence of lower kinetics intercalation reactions in compassion with that ITP of SA. In both the electrolytic cases, the η increases with an increase in current densities and reaches 100 % at higher current densities (Figure. 5e). The cyclic stability of PZnSn was evaluated ITP of both the electrolytes at 0.4 V s^{-1} (Figure. 5f).

The change of Q (Eqn. S1) as a function of INC exhibits a trend of peaks and valleys in the cases of both the electrolytes, and the extent of peaks and valleys is lower in the case of SLP, which indicates more compatibility than the SLP has with PZnSn. This stability ITP of SLP also signifies the robustness and reversibility of energy storage reactions of PZnSn ITP of SLP. However, an overall increase in Q is observed (Figure. 5f). During the cyclic stability test, the consecutive increase and decrease of Q is attributed to the simultaneous structural breakdown and self-healing

View Article Online
DOI: 10.1039/D4YA00617H

of emaraldine salt form of PANI [58]. The reason for an increase in *Q* with INC is that the continuous insertion and extraction of ions of SA and SLP increase the intercalation processes of the PZnSn. This increase in intercalation processes is the main reason for the increase in *Q* with INC. This intercalation process occurs until the electrode material is structurally damaged. This continuous diffusion of electrolytes unite the discrete parts of the PZnSn, and thus, the surface of electrode material that takes part in energy storage increases. Once the material damage occurs, the extent of energy storage reactions decreases, leading a reduction in the amount of energy stored. The peak and valley trend observed in the *Q* with INC (Fig. 5f) is due to the simultaneous structural breakdown and self-healing of emaraldine salt form of PANI[58]. Once the self-healing property of PANI is ceased, the continuous decrease in *Q* is observed due to the complete conversion of all emaraldine (half reduced and half oxidized form) to pernigraniline (completely oxidized form)[20]. The plots of *b*-value *vs*. potential of PZnSn obtained ITP of SA (Figure. 6a) and SLP (Figure. 6b), obtained after DNC, substantiate this rationalism.

View Article Online
DOI: 10.1039/D4YA00617H

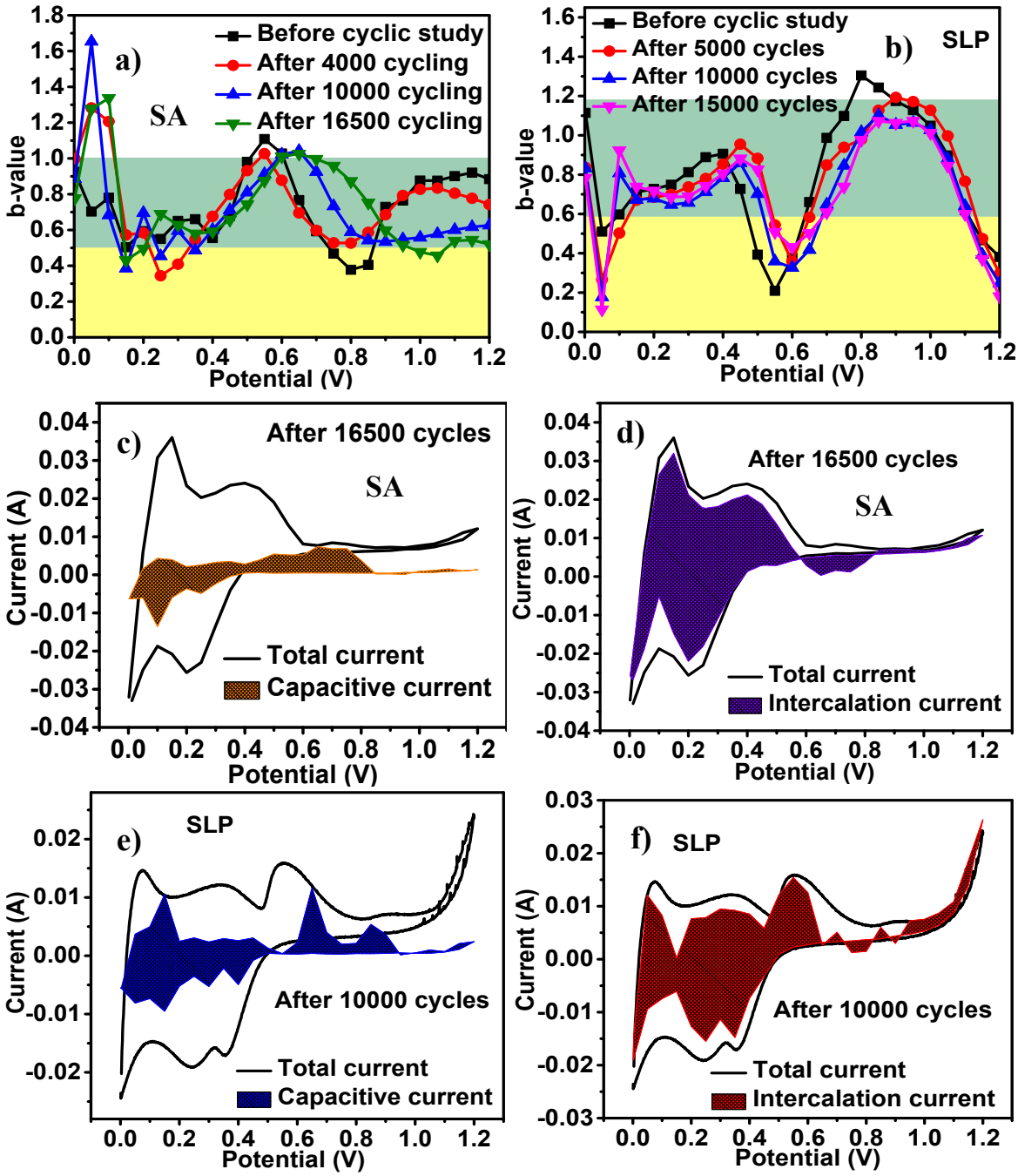

Figure 6. The plots of *b*-values *vs.* potential of PZnSn ITP of a) SA & b) SLP after DNC. The deconvolution of the CV curve of PZnSn ITP SA was obtained after 16,500 cycles providing c) capacitive current and d) intercalation current. The deconvolution of the CV curve of PZnSn ITP SLP was obtained after 10,000 cycles providing e) capacitive current and f) intercalation current.

View Article Online
DOI: 10.1039/D4YA00617H

The comparison of plots of *b*-values *vs*. potential (Figure.6a and Figure.6b) and CV curves that are attained after DNC ITP of SA (Figure. S7) and SLP (Figure. S8) evidently depict that the intense peaks that are present in CV profiles of PZnSn ITP of both the electrolytes are due to the intercalation processes, as they possess *b*-values (Eqn. S8) closer to 0.5. In addition, with INC, the current produced by these intercalation peaks increases, indicating the enhanced occurrence of intercalation processes. Since the intercalation process is bulk, it stores higher energy than redox reactions and the EDL formation process, which are surface phenomena. With INC, the quasi-reversibility of the faradaic reactions increases, and this quasi-reversibility is attributed to the structural breakdown of PZnSn, which causes internal resistance. Because of this quasi-reversibility and internal resistance, the η decreases with INC in the cases of both the electrolytes. This above-mentioned internal resistance is seen in the form of increased IR drop with INC, which is to be discussed in successive sections.

The deconvolution of CV curves that are obtained after 16,500 cycles and 10,000 cycles ITP of SA (Figure. 6c and 6d) and SLP (Figure. 6e and 5f), respectively, provide the percentage of energy stored by capacitive processes (Eqn. S7) (EDL + redox reaction) and intercalation reactions as 27.17 and 72.83%; and 21 and 79%, respectively. In the case of SA, the percentages of intercalation reaction are increased with INC as indicated by the quantity of intercalation contribution after 16,500 cycles, whereas, in the case of SLP, the percentage of capacitive and intercalation contributions are intact in quantity; however, their magnitudes are increase as indicated by the migration of *b*-values closer to the value of 0.5 (Figure.6b) and increase of intensities of CV peaks with INC. This combined occurrence of all three energy storage processes, EDL formation, redox reaction and intercalation reactions, relatively to a higher extent, ITP of SLP is fetching the higher energy storage in its presence in PZnSn, in relation to that ITP of SA.

View Article Online
DOI: 10.1039/D4YA00617H

As seen in Figure. 6a and 6b, with INC, the potential range involved in the intercalation reaction increases; thus, the potential regions that are involved in the intercalation reaction are 0-0.4 V (Figure. 6a) and 0 - 0.8 V (Figure. 6b) in the cases of SA and SLP, respectively. This long-order intercalation reaction ITP of SLP fetches higher energy storage in PZnSn in its presence.

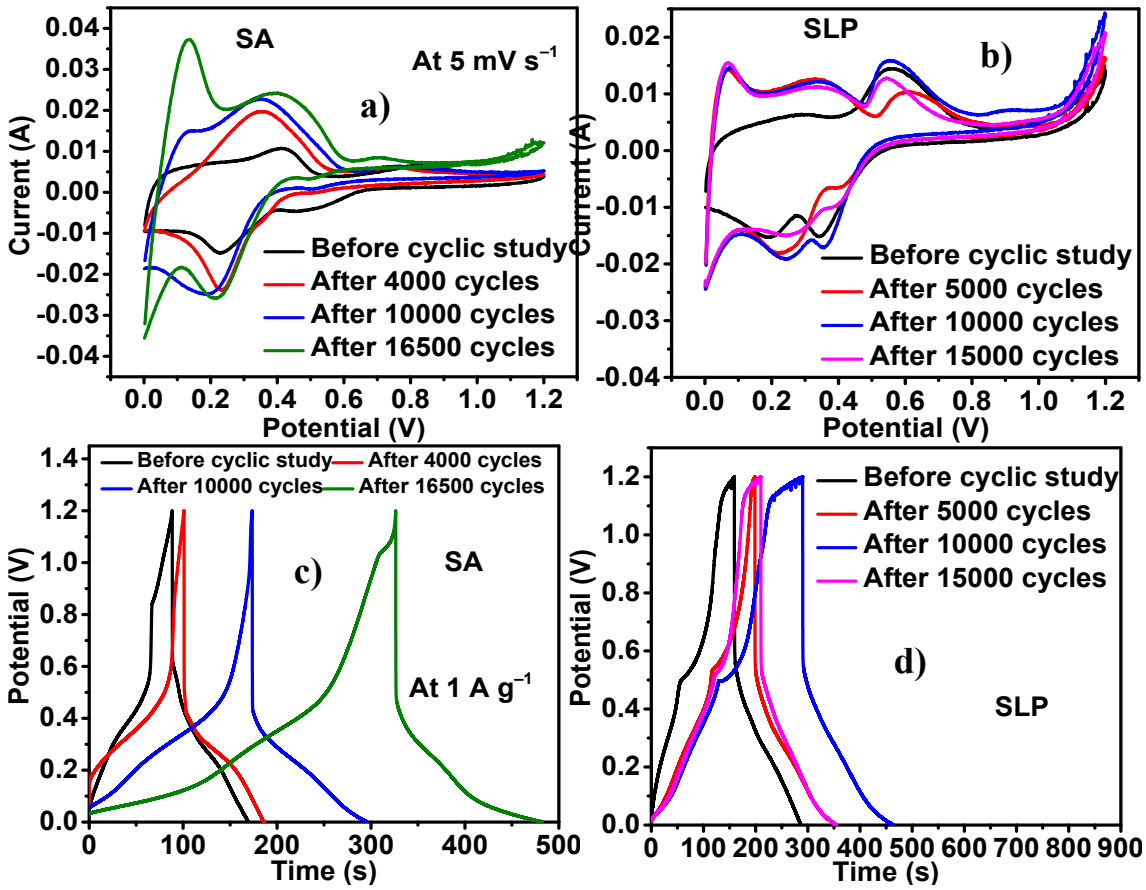

Figure 7. CV plots of PZnSn after DNC at 5 mV s^{-1} ITP of a) SA & b) SLP. The CD plots of PZnSn after DNC at 1 A g^{-1} ITP of c) SA & d) SLP.

The increase of area of faradaic peaks and discharge time (t_d) of CV curves (Figure. 7a and Figure. 7b) and discharge curves (Figure.7c and Figure. 7d), respectively, of PZnSn ITP of SA and SLP obtained after DNC indicate the increase of energy storage with INC. The high CV area and

View Article Online
DOI: 10.1039/D4YA00617H

t_d (Figure. S9a and Figure. S9b) of PZnSn obtained after 16,500 and 10,000 cycles indicate the maximum energy stored in it after 16,500 and 10,000 cycles ITP of SA and SLP, respectively.

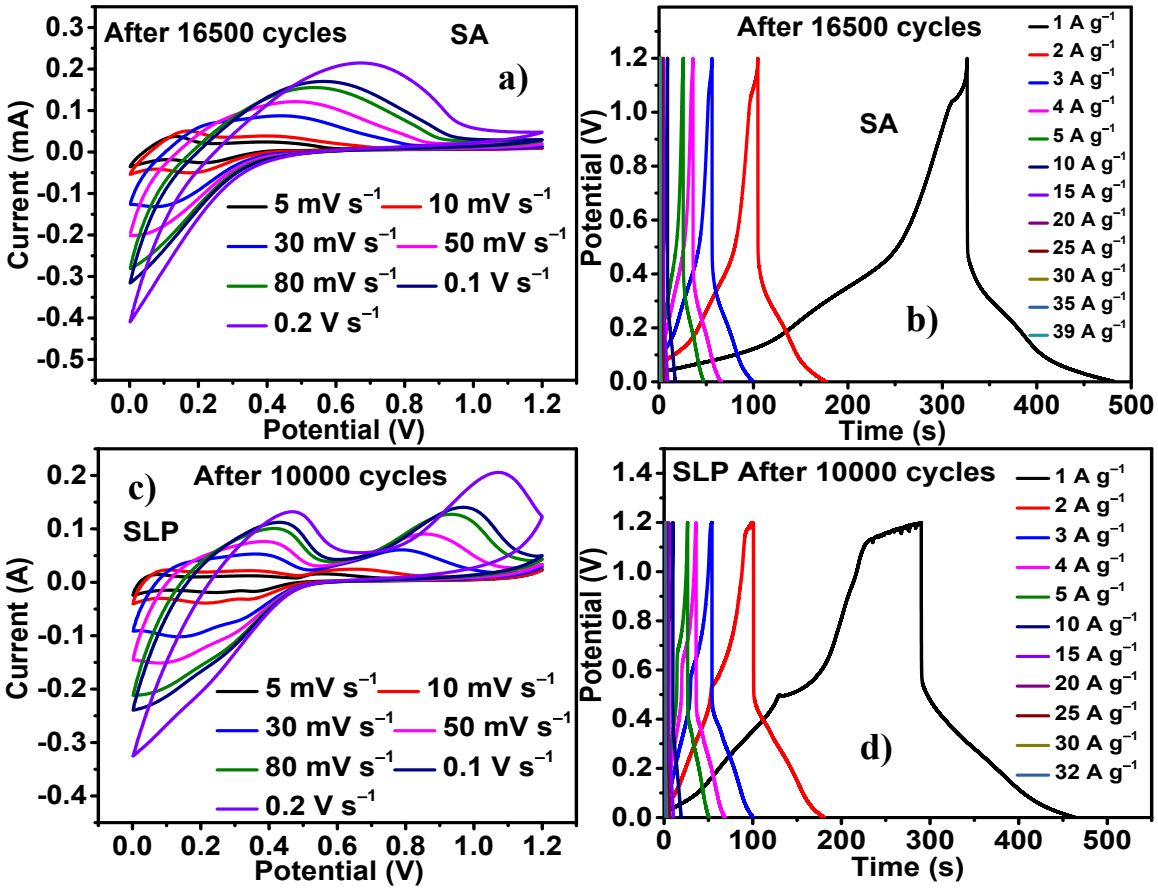

Figure 8. a) CV plots at different scan rates and b) CD plots at different current densities of PZnSn after 16,500 cycles ITP of SA, c) CV plots at different scan rates, and d) CD plots at different current densities of PZnSn after 10,000 cycles ITP of SLP.

The sustainability of the PZnSn to the high applied potential and current, even after 16,500 cycles (Figure. 8a and Figure. 8b) and 10,000 cycles (Figure.8c and Figure. 8d) ITP of SA and SLP, respectively, is evident. The PZnSn consistently exhibits the faradaic nature even up to 0.2 V s^{-1} and 39 A g^{-1} in the case of SA and up to 0.2 V s^{-1} and 32 A g^{-1} in the case of SLP. It is to be remarked that after 5000 cycles, the PZnSn is consistent in exhibiting a faradaic nature up to 42 A

View Article Online
DOI: 10.1039/D4YA00617H

g^{-1}, which is the highest current tolerance obtained ITP of SLP. This decrease in current tolerance exhibited by PZnSn ITP of SLP after 10,000 cycles indicates the increase of quasi reversibility of energy storage reactions and increase of diffusional resistance due to the slight structural deformation in PZnSn with INC. The IR drop observed after 0, 4000, 10,000, and 16,500 cycles ITP of SA are 0.2735, 0.3477, 0.3456 and 0.2741 V, respectively. Similarly, the IR drop observed after fresh cell, 5000, 10,000, and 15,000 cycles ITP of SLP are 0.17, 0.22, 0.21 and 0.22 V, respectively. These increasing trends of IR drops in both cases are not so significant; therefore, the tradeoff between the slight structural deformation and the continuous enhancement of diffusion of electrolytes causing the increase in intercalation reactions and bringing higher energy storage with INC is implied. The relatively low IR drop exhibited by PZnSn ITP of SLP indicates the enhanced conductivity and better diffusion of ions of SLP into PZnSn in comparison with that of SA.

Figure. 9a depicts the increase of *Q*, sustainability to applied current and rate capability of PZnSn with INC ITP of SA. The *Q* obtained ITP SA at 1 A g^{-1} before cyclic study; after 4000, 10,000 and 16,500 cycles are 162, 169, 243, and 312 C g^{-1}, respectively. The maximum current tolerance exhibited by PZnSn ITP SA before the cyclic stability study after 4000, 10,000 and 16,500 cycles are 14, 25, 28 and 39 A g^{-1}, respectively. The retention of initial *Q* exhibited by the PZnSn ITP SA at 14 A g^{-1} are 17.28, 44.88, 43.86 and 45.23%, before the cyclic stability study, after 4000, 10,000 and 16,500 cycles. The retention of initial *Q* exhibited by the PZnSn ITP of SA at the maximum current densities of 25, 28, and 39 A g^{-1} are 28.88, 23.43 and 12% after 4000, 10,000 and 16,500 cycles, respectively. The increase in *Q* and the rate capability is attributed to the higher magnitude of porosities present on the surface of PZnSn, causing better electrolyte permeation into the PZnSn with INC and enabling promising diffusion of electrolyte into PZnSn even at higher current densities as it occurs at lower current densities. The plots of *E* vs *P* (Figure. 8b) possess a

View Article Online
DOI: 10.1039/D4YA00617H

similar trend as that of Figure. 8a. The maximum *E* obtained from PZnSn ITP of SA at 1 A g^{-1} and at a *P* of 1.2 kW kg^{-1} are 27.01, 28.28, 40.64 and 52 Wh kg^{-1} before cyclic study, after 4000, 10,000 and 16,500 cycles, respectively.

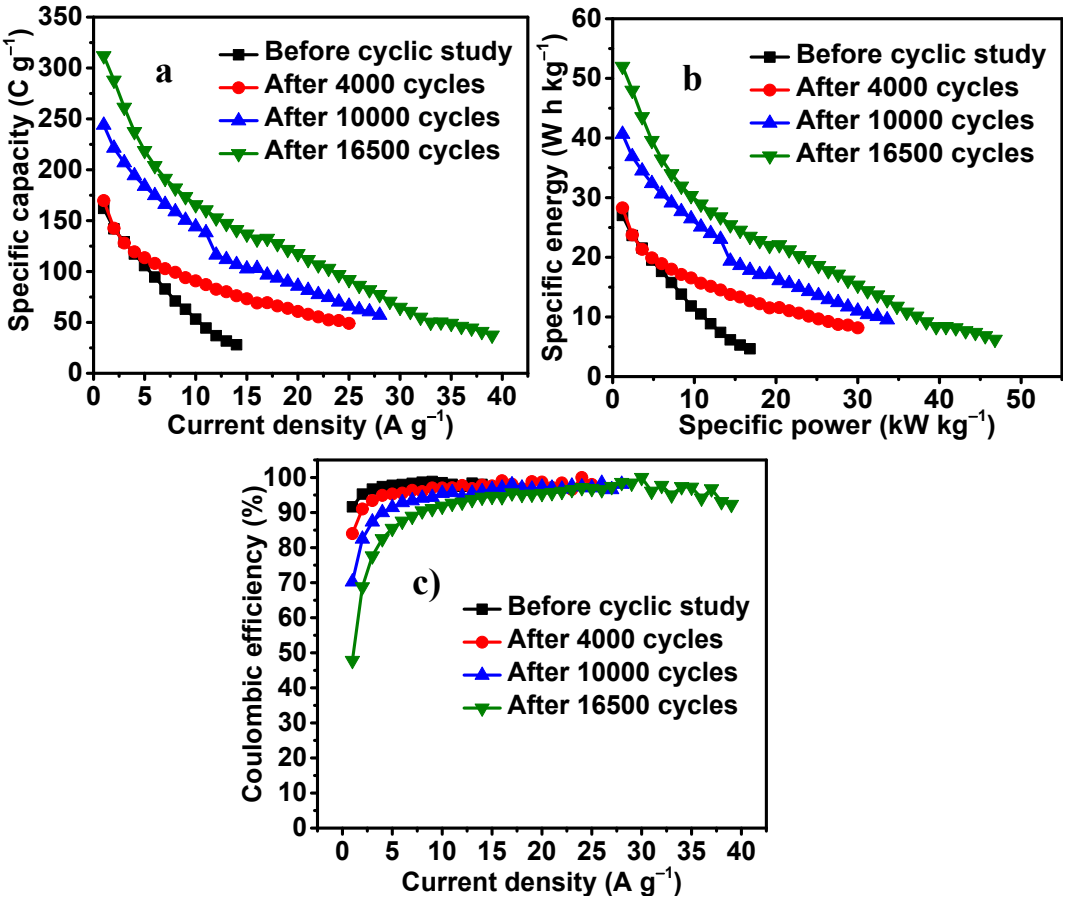

Figure 9. Plots of a) specific capacity vs current density, b) specific energy *vs.* specific power, and c) columbic efficiency *vs.* current density of PZnSn obtained after DNC ITP of SA.

The η (Figure. 8c) obtained from PZnSn ITP of SA at 1 A g^{-1} are 93.63, 84.02, 70.24 and 47.81%, before the cyclic study, after 4000, 10,000 and 16,500 cycles, respectively. As the current density increases, the η also increases and reaches the maximum of 100% at higher current densities during all points of cycling. The decrease of η with INC is ascribed to the increase in the

View Article Online
DOI: 10.1039/D4YA00617H

extent of intercalation processes, whose kinetics is lower than that of surface capacitive processes and the increase of quasi-reversibility of the energy storage processes. After 16,500 cycles, the

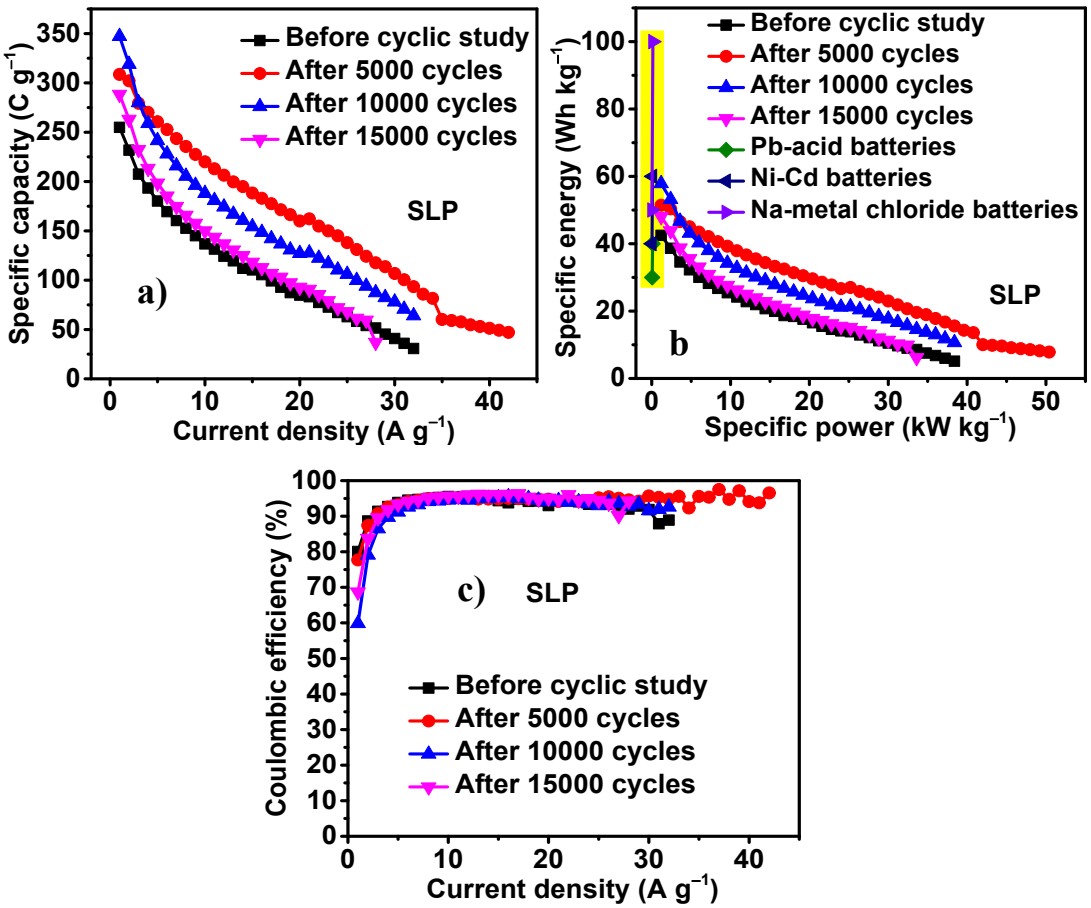

obtained η is minimum, which indicates the occurrence of a greater extent of intercalation, higher energy storage caused by it and higher quasi-reversibility. This quasi-reversibility is seen in the form of *b*-values with a magnitude of more than one at lower potentials (Figure. 6a), and that region corresponds to the intercalation processes (Figure. 6d).

Figure 10. Plots of a) specific capacity *vs.* current density, b) specific energy *vs.* specific power, and c) columbic efficiency *vs.* current density of PZnSn obtained after DNC ITP of SLP.

View Article Online
DOI: 10.1039/D4YA00617H

Figure. 10a depicts the increase of *Q*, sustainability to applied current and rate capability of PZnSn with INC ITP of SLP. The *Q* obtained ITP SLP at 1 A g^{-1} before the cyclic study; after 5000, 10,000 and 15,000 cycles are 255, 309, 347, and 288 C g^{-1}, respectively. The maximum current tolerance exhibited by PZnSn ITP SLP before the cyclic stability study, after 5000, 10,000 and 15,000 cycles, are 32, 42, 32 and 28 A g^{-1}, respectively. The retention of initial *Q* exhibited by the PZnSn ITP SLP at 28 A g^{-1} is 20.21, 38.11, 25.16 and 12.82% before the cyclic stability study, after 5000, 10,000 and 15,000 cycles, respectively. The retention of initial *Q* exhibited by the PZnSn ITP of SLP at the maximum current densities of 32, 42, and 32 A g^{-1} are 12.05, 15.24 and 18.43% before the cyclic study, after 5000 and 10,000 cycles, respectively. The increase in *Q* and the rate capability ITP of SLP in relation to SA is attributed to the higher electrolyte permeation into the PZnSn with INC and enabling promising diffusion of electrolyte into the pores of PZnSn even at higher current densities as it occurs at lower current densities in comparison with SA. The plots of *E vs*. *P* (Figure. 10b) possess a similar trend as that of Figure. 10a. The maximum *E* obtained from PZnSn ITP of SLP at 1 A g^{-1} and at a *P* of 1.2 kW kg^{-1} are 42.49, 51.43, 57.86 (comparable with Ni-Cd batteries) and 48.06 Wh kg^{-1} before cyclic study, after 5000, 10,000 and 15,000 cycles, respectively. The η (Figure. 10c) obtained from PZnSn ITP of SLP at 1 A g^{-1} are 80.07, 77.69, 59.84 and 68.68 % before cyclic study after 5000, 10,000 and 15,000 cycles. The overall low η of PZnSn ITP of SLP in comparison with that ITP of SA is attributed to the occurrence of higher extent low kinetic intercalation reaction ITP of SLP. In both the cases of SA (Figure. 9c) and SLP (Figure. 10c), as the current density increases, the η also increases and reaches the maximum of 100% at higher current densities during all points of cycling.

All the Nyquist plots of PZnSn obtained ITP SA(Figure. 11a) contain a semi-circle at a higher frequency region (HFR) and a linear Warburg portion at a lower frequency region (LFR),

View Article Online
DOI: 10.1039/D4YA00617H

indicating the capacitive behavior of the PZnSn ITP SA. The resistance along the real axis of the Nyquist plots is associated with the series resistance of the PZnSn. The series resistance is the cumulative of the solution resistance (R_s), charge-transfer resistance (R_{ct}), and Warburg diffusional resistance (W). This series resistance decreases with INC, indicating a reduction in overall resistance with INC ITP SA.

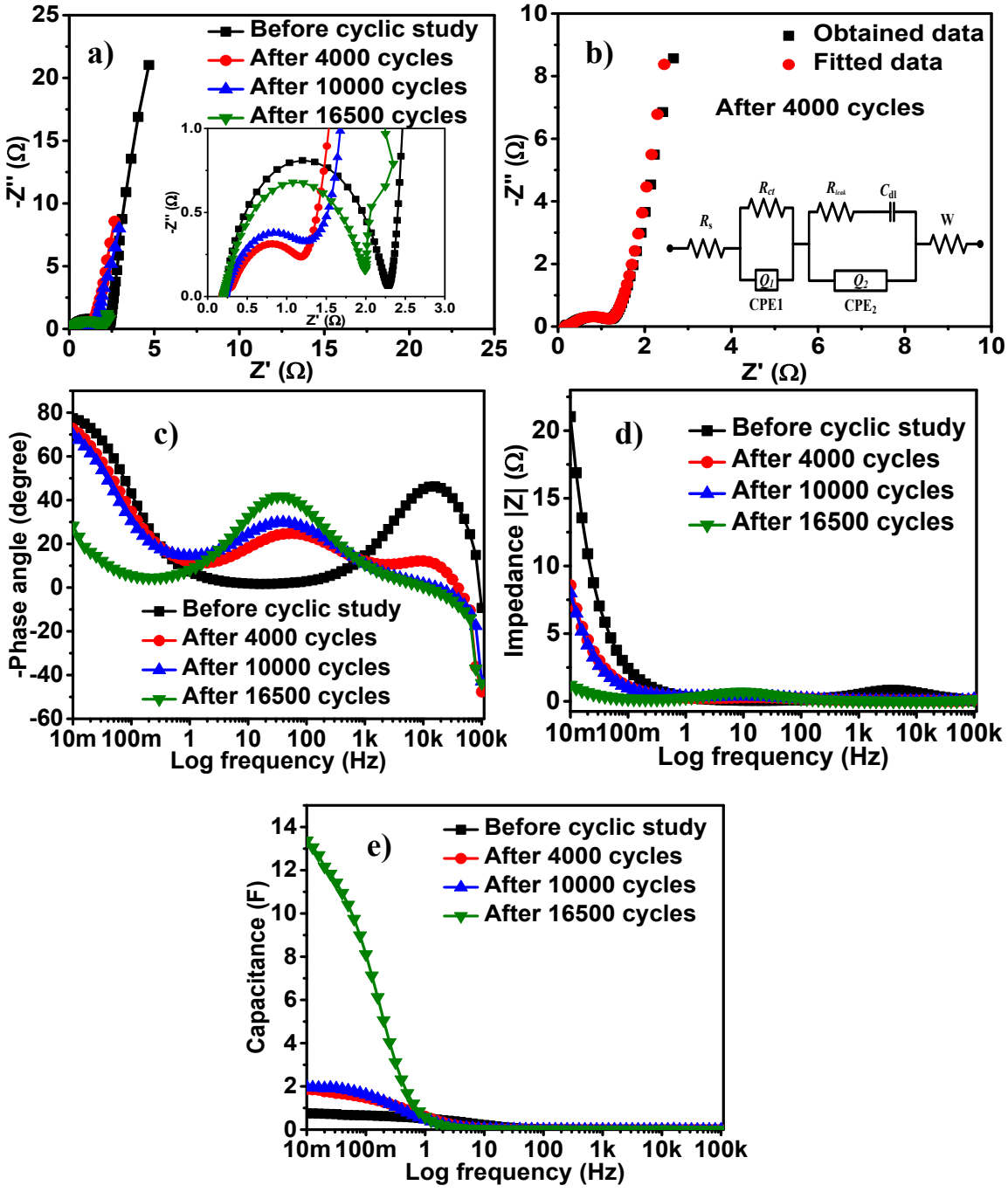

View Article Online
DOI: 10.1039/D4YA00617H

Figure 11. a) Nyquist plot, b) EC fitment to Nyquist plot obtained after 4000 cycles, c)Bode phase angle plots, d) Bode impedance plots and e) capacitance *vs.* log frequency plots of PZnSn obtained after DNC ITP SA.

Table 4 The magnitudes of electrical parameters of PZnSn composites obtained ITP of SA by equivalent circuit fitment of $R_s(R_{ct}Q_1)((R_{leak}C_{dl})(Q_2))W$.

PZnSn	R_s (Ω)	R_{ct} (Ω)	Q_1 (F)	n_1	R_{leak} (Ω)	C_{dl} (F)	Q_2 (F)	n_2	W (Ω)
Before cyclic study	0.23	0.01	$8.52\times E^{-14}$	0.80	2.10	0.79	$1.18\times E^{-4}$	0.82	2.33
After 4000 cycles	0.19	0.3	$2.10\times E^{-3}$	0.57	0.90	2.14	0.0358	0.71	2.35
After 10,000 cycles	0.21	1.13	0.0483	0.69	0.18	2.43	$6.22\times E^{-6}$	0.99	2.53
After 16,500 cycles	0.20	1.77	0.0203	0.82	0.21	17.23	$5.49\times E^{-6}$	0.99	11.38

Table 5 The magnitudes of electrical parameters of PZnSn composites obtained ITP of SLP by equivalent circuit fitment of $R_s(R_{ct}Q_1)((R_{leak}C_{dl})(Q_2))W$.

PZnSn	R_s (Ω)	R_{ct} (Ω)	Q_1 (F)	n_1	R_{leak} (Ω)	C_{dl} (F)	Q_2 (F)	n_2	W (Ω)
Before cyclic study	0.20	0.56	0.01	0.59	0.24	1.02	$3.15\times E^{-2}$	0.35	4.45
After 5000 cycles	0.20	0.26	0.79	0.47	0.37	1.40	$7.20\times E^{-4}$	0.47	2.19
After 10,000 cycles	0.25	0.08	1.25	0.64	0.37	1.20	$3.35\times E^{-3}$	0.62	2.13
After 15,000 cycles	0.31	0.22	0.45	0.99	0.66	1.01	$3.69\times E^{-2}$	0.35	2.19

View Article Online
DOI: 10.1039/D4YA00617H

The magnitudes of electrical elements involved in the energy storage processes are attained by the fitment of equivalent circuit (EC) $R_s(R_{ct}Q_1)((R_{leak}C_{dl})(Q_2))W$ (Table 4) (Figure. 11b) to Nyquist plots obtained ITP SA, indicate that with INC the R_s is decreasing; and R_{ct}, C_{dl} and W are increasing. The explanations of electrical elements present in EC are provided in supporting information. The decrease in R_s and increase in C_{dl} are attributed to the enhancement of energy storage with INC. The increase of R_{ct} and W are accounted for the increase of IR drop with INC and the reduction in the η with INC ITP of SA, respectively. The lower IR drop obtained before the cyclic stability study ITP of SA in relation to other points in the cyclic stability study is associated with its low R_{ct}. The increase of W with INC indicates the increase of resistance against the diffusion of electrolytic ions with INC, and this resistance is the reason behind the decrease of η with INC ITP SA. The Bode Phase angles (Figure. 11c) at LFR decrease with INC, indicating the migration from the state of capacitor behavior to supercapacitor behavior. The relaxation time (τ_o) (Eqn. S10) of PZnSn obtained before the cyclic study, after 4000 and 10,000 cycles are 0.81, 0.87 and 0.89 s, respectively. The phase angle plot obtained after 16,500 cycles did not reach the phase angle of –45°, and therefore, the τ_o after 16,500 cycles was left uncalculated. The increase of τ_o indicates the increase in energy storage with INC. The variation of Bode impedance plots obtained ITP of SA (Figure. 11d) with INC is in agreement with the variation of series resistance with INC. The decrease in overall resistance resulted in overall increase of energy storage with INC (Figure. 9e). The impedance and capacitance (Eqn. S11) obtained ITP of SA at LFR of 0.01 Hz are 21.03, 8.57, 8.0, and 1.19 Ω; and 0.76, 1.86, 1.99, and 13.38 F, before cyclic study, after 4000, 10,000 and 16,500 cycles, respectively.

View Article Online
DOI: 10.1039/D4YA00617H

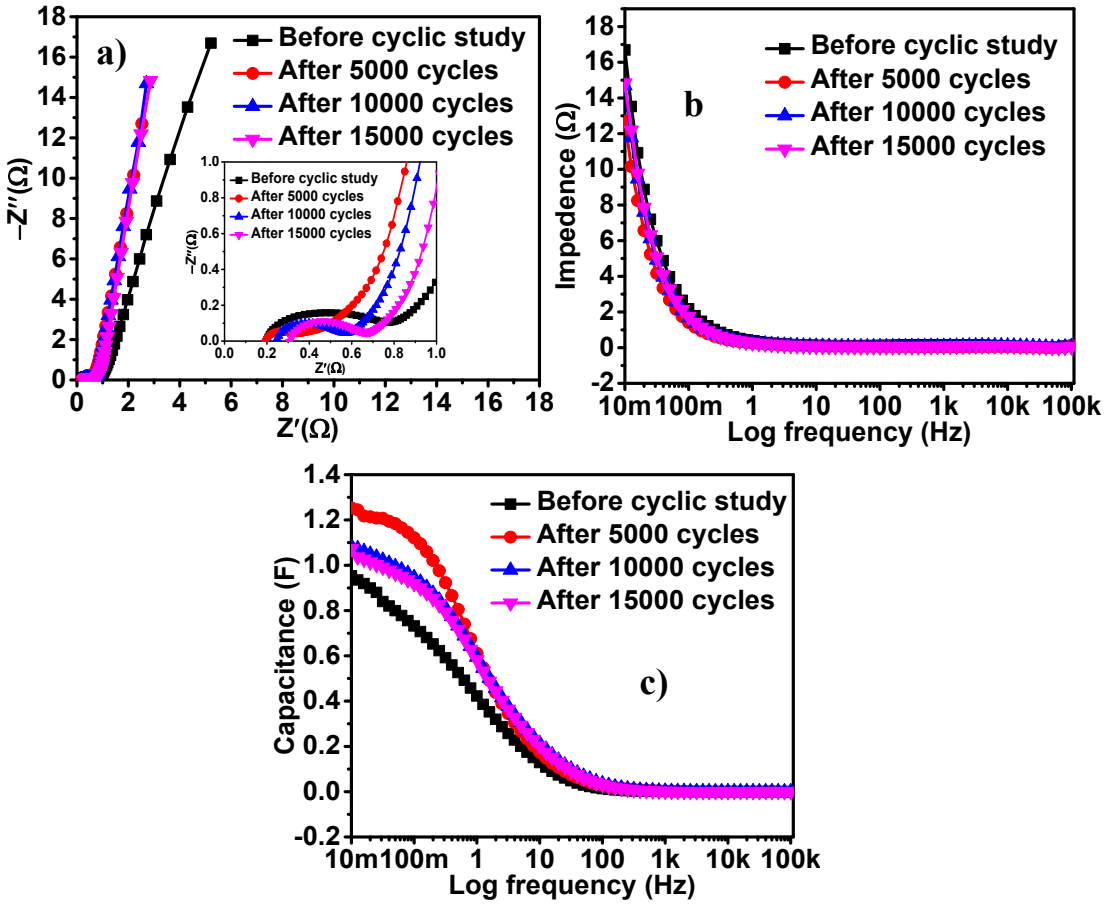

Figure 12. a) Nyquist plots, b) Bode impedance plots and d) capacitance *vs.* log frequency plots of PZnSn obtained after DNC ITP SLP.

Similarly, the EIS results of PZnSn ITP of SLP (Figure.12) depict the decreased resistance (Figure. 12a) with INC, indicating the better diffusion of electrolytic ions and increased energy storage with INC ITP of SLP. However, it is intriguing to note that the maximum performance was obtained after 10,000 ITP of SLP, but impedance (Figure. 12b) and the capacitance (Figure.12c) corresponding to the EIS analysis after 5000 cycles are found to be the least and highest, respectively. This puzzle could be understood when the charge storage characters obtained after 5000 and 10,000 cycles ITP of SLP cycles are compared. That is, the higher energy storage obtained after 10,000 cycles holds true only up to 3 A g^{-1}, after which all the Q that are obtained

View Article Online
DOI: 10.1039/D4YA00617H

after 10,000 cycles are lower than that obtained after 5000 cycles. In addition, the rate capability and the tolerance to the higher current are found to be superior after 5000 cycles. Therefore, it is rational that PZnSn experiences lower impedance and stores higher energy after 5000 cycles ITP of SLP, which is seen in the EIS results of PZnSn obtained ITP of SLP. The magnitudes of electrical elements that are obtained by fitting the same EC to the Nyquist plots of PZnSn that are obtained ITP of SLP after DNC (Table 5) evidently depict that with INC, the overall resistances are decreasing, the overall capacitances are increasing, and the least resistance and maximum capacitance are obtained after 5000 cycles. The rate capability and the coulombic efficiencies follow the same trend as that of *W* obtained after DNC. The PZnSn exhibits maximum rate capability after 5000 cycles, as it possesses the least *W* at that point ITP of SLP.

In order to study the contributions and nature of electrolytes used, their EIS studies were carried out by making devices that contain electrolytes (SA and SLP), separator and current collector without electrode material, and the findings are displayed in Figure. S10. As seen, the Nyquist plots have the distorted semicircle and a Warburg (Figure.S10a) showing the double layer formation at the solid (separator and current collector) and liquid (electrolytes) interface. The Bode impedance plots (Figure.S10b) and log frequency vs capacitance plots (Figure.S10c) show that the SLP exhibits lower impedance and higher capacitance ITP of SLP, signifying its superiority to SA. The obtained impedance and capacitance ITP of SA and SLP are 4.862 and 4.127 kΩ; and 3.27 and 3.86 mF, respectively, at 0.01 Hz. The open circuit potential (OCP) obtained for these electrodeless devices are 167.4 mV and 206.7 mV ITP of SA and SLP, respectively. This high OCP obtained ITP of SLP indicates its lower internal resistance and higher ability to store energy in relation to that ITP of SA. Thus, the higher energy storage ITP of SLP is substantiated. The

View Article Online
DOI: 10.1039/D4YA00617H

comparable performance of PZnSn with the reported ones is seen in Table 6, and the obtained results are comparable and even better than some of the reports published elsewhere.

Table 6 Comparison of energy storage performance of PZnSn with similar composites.

Composite	Electrolyte	Potential window (V)	*E* (Wh kg^{-1})	*P* (kW kg^{-1})	Cyclic stability	Ref.
2-EL systems						
PANI/ZnO/VO_2	1 M H_2SO_4	1.2	88.10 at 1 A g^{-1}	2.154	Good cyclic stability up to 16,812 cycles at 0.4 A g^{-1}	5
PANI/CuO/NiO	0.1 M Na_2SO_4	1.6	35.0 at 3.5 A g^{-1}	1.326	86% retention up to 10000 cycles	59
PANI/CuO/SnO_2	1 M H_2SO_4	1.2	42.73 at 1 A g^{-1}	1.200	45.64% up retention to 5000 cycles at 0.4 V s^{-1}	44
PANI/CuO/SnO_2	1 M H_2SO_4 + 1 M CH_3SO_3H (1:1)	1.2	50.26 at 1 A g^{-1}	1.200	55.56% retention up to 12500 cycles at 0.4 V s^{-1}	44
Present work PANI/ZnO/SnO_2	1 M H_2SO_4	1.2	52.00 at 1 A g^{-1}	1.200	No deterioration up to 16,500-cycles at 0.4 V s^{-1}	
Present work PANI/ZnO/SnO_2	By-product of PANI	1.2	57.87 at 1 A g^{-1}	1.200	No deterioration up to 15,000-cycles at 0.4 V s^{-1}	
3-EL systems						
PANI/Y_2O_3-ZnO	1 M KOH	1.0	73.08	9.135	94.9% retention up to 5000 cycles	60

View Article Online
DOI: 10.1039/D4YA00617H

PANI/Ag-ZnO	1 M H_2SO_4	0.8	88.00	0.4990	-	[61]

CONCLUSION

A composite, polyaniline/ZnO/SnO_2 of weight percentages of 58.34%: 8.33%:33.33% (PZnSn), respectively, was synthesized in a facile *in-situ* single-step method. The energy storage performance was evaluated with two aqueous electrolytes, viz., 1 M H_2SO_4 (SA) and the liquid by-product that was obtained after the synthesis of PANI (SLP). The SLP provided 57.25% higher energy storage performance in relation to that provided by the SA. The PZnSn exhibited a durable and rate-capable energy storage property by exhibiting robustness up to 16500 cycles at 0.4 V s^{-1} and 39 A g^{-1}, respectively, in the presence (ITP) of SA and up to 15,000 cycles at 0.4 V s^{-1} and 42 A g^{-1} ITP of SLP, respectively, in a real-time symmetric two electrode systems. The PZnSn displayed a remarkable trait of energy storage enhancement with an increase in charge and discharge cycles ITP of both the electrolytes. However, the enhancement provided by SLP is higher than that of SA. The maximum performance achieved from PZnSn ITP of SLP is a *Q* of 347 C g^{-1}, an *E* of 57.87 Wh kg^{-1} (comparable with Ni-Cd batteries) and a *P* of 1.2 kW kg^{-1} at 1 A g^{-1}. Therefore, the PZnSn ITP of SLP would be suitable for fabricating hybrid supercapacitors that provide high energy, high rate capability, and durability. The use of SLP in energy storage brings the entire work under the umbrella of "waste into wealth" and the concept of "green energy storage".

ASSOCIATED CONTENTS

Supporting information

View Article Online
DOI: 10.1039/D4YA00617H

Synthesis of PANI and its by-product (S1), Characterization details (S2), Fabrication details (S3), Fig. S1, Fig. S2, Fig. S3, Fig. S4, Fig. S5, FT-IR Spectrum of PZnSn (F4), Formulae used (S5) (Eqn. S1-S8), Fig. S6, Fig. S7, Fig. S8, Fig. S9, Fig. S10, Descriptions of electrical elements of equivalent circuit (S6), Eqn. S9-S11.

Acknowledgment

Dr Aranganathan Viswanathan (AV) acknowledges the financial support provided by the Science and Engineering Research Board (SERB), India, in the form of a National Post-Doctoral Fellowship (PDF/2023/000769). VA acknowledges financial support from the Anusandhan National Research Foundation (ANRF), Govt. of India, through Swarnajayanti Fellowship (SB/SJF/2020-21/12).

REFERENCES

(1) Chen, W.; B. Rakhi, R.; N. Alshareef, H. Facile Synthesis of Polyaniline Nanotubes Using Reactive Oxide Templates for High Energy Density Pseudocapacitors. *J. Mater. Chem. A* **2013**, *1* (10), 3315–3324. https://doi.org/10.1039/C3TA00499F.

(2) Liu, T.; Finn, L.; Yu, M.; Wang, H.; Zhai, T.; Lu, X.; Tong, Y.; Li, Y. Polyaniline and Polypyrrole Pseudocapacitor Electrodes with Excellent Cycling Stability. *Nano Lett.* **2014**, *14* (5), 2522–2527. https://doi.org/10.1021/nl500255v.

(3) Viswanathan, A.; Shetty, A. N. Influence of Different Dopants and Redox Forms of PANI in Its Crystal Structure, Morphology, Electrochemical Energy Storage to Variable Extent, Unique Properties and Kinetics. *Bull. Mater. Sci.* **2022**, *45* (2), 60. https://doi.org/10.1007/s12034-021-02626-9.

View Article Online
DOI: 10.1039/D4YA00617H

(4) Chen, Y.; Manzhos, S. Voltage and Capacity Control of Polyaniline Based Organic Cathodes: An Ab Initio Study. *J. Power Sources* **2016**, *336*, 126–131. https://doi.org/10.1016/j.jpowsour.2016.10.066.

(5) Viswanathan, A.; Shetty, A. N. Nanoporous PANI/ZnO/VO2 Ternary Nanocomposite and Its Electrolyte for Green Supercapacitance. *Mater. Sci. Eng. B* **2024**, *303*, 117322. https://doi.org/10.1016/j.mseb.2024.117322.

(6) Huang, B.; Li, X.; Pei, Y.; Li, S.; Cao, X.; Massé, R. C.; Cao, G. Novel Carbon-Encapsulated Porous SnO2 Anode for Lithium-Ion Batteries with Much Improved Cyclic Stability. *Small* **2016**, *12* (14), 1945–1955. https://doi.org/10.1002/smll.201503419.

(7) Hwang, S. M.; Lim, Y.-G.; Kim, J.-G.; Heo, Y.-U.; Lim, J. H.; Yamauchi, Y.; Park, M.-S.; Kim, Y.-J.; Dou, S. X.; Kim, J. H. A Case Study on Fibrous Porous SnO2 Anode for Robust, High-Capacity Lithium-Ion Batteries. *Nano Energy* **2014**, *10*, 53–62. https://doi.org/10.1016/j.nanoen.2014.08.020.

(8) Deng, Y.; Fang, C.; Chen, G. The Developments of SnO2/Graphene Nanocomposites as Anode Materials for High Performance Lithium Ion Batteries: A Review. *J. Power Sources* **2016**, *304*, 81–101. https://doi.org/10.1016/j.jpowsour.2015.11.017.

(9) Li, Z.; Gong, L. Research Progress on Applications of Polyaniline (PANI) for Electrochemical Energy Storage and Conversion. *Materials* **2020**, *13* (3), 548. https://doi.org/10.3390/ma13030548.

(10) Hsieh, C.-T.; Lin, C.-Y.; Chen, Y.-F.; Lin, J.-S. Synthesis of ZnO@Graphene Composites as Anode Materials for Lithium Ion Batteries. *Electrochimica Acta* **2013**, *111*, 359–365. https://doi.org/10.1016/j.electacta.2013.07.197.

View Article Online
DOI: 10.1039/D4YA00617H

(11) Zhang, C. Q.; Tu, J. P.; Yuan, Y. F.; Huang, X. H.; Chen, X. T.; Mao, F. Electrochemical Performances of Ni-Coated ZnO as an Anode Material for Lithium-Ion Batteries. *J. Electrochem. Soc.* **2006**, *154* (2), A65. https://doi.org/10.1149/1.2400609.

(12) Huang, X. H.; Xia, X. H.; Yuan, Y. F.; Zhou, F. Porous ZnO Nanosheets Grown on Copper Substrates as Anodes for Lithium Ion Batteries. *Electrochimica Acta* **2011**, *56* (14), 4960–4965. https://doi.org/10.1016/j.electacta.2011.03.129.

(13) Zhang, J.; Gu, P.; Xu, J.; Xue, H.; Pang, H. High Performance of Electrochemical Lithium Storage Batteries: ZnO-Based Nanomaterials for Lithium-Ion and Lithium–Sulfur Batteries. *Nanoscale* **2016**, *8* (44), 18578–18595. https://doi.org/10.1039/C6NR07207K.

(14) Purushothaman, K. K.; Priya, V. S.; Nagamuthu, S.; Vijayakumar, S.; Muralidharan, G. Synthesising of ZnO Nanopetals for Supercapacitor Applications. *Micro Amp Nano Lett.* **2011**, *6* (8), 668–670. https://doi.org/10.1049/mnl.2011.0260.

(15) Saranya, M.; Ramachandran, R.; Wang, F. Graphene-Zinc Oxide (G-ZnO) Nanocomposite for Electrochemical Supercapacitor Applications. *J. Sci. Adv. Mater. Devices* **2016**, *1* (4), 454–460. https://doi.org/10.1016/j.jsamd.2016.10.001.

(16) Mohapatra, D.; Parida, S.; Badrayyana, S.; Singh, B. K. High Performance Flexible Asymmetric CNO-ZnO//ZnO Supercapacitor with an Operating Voltage of 1.8 V in Aqueous Medium. *Appl. Mater. Today* **2017**, *7*, 212–221. https://doi.org/10.1016/j.apmt.2017.03.006.

(17) Kalpana, D.; Omkumar, K. S.; Kumar, S. S.; Renganathan, N. G. A Novel High Power Symmetric ZnO/Carbon Aerogel Composite Electrode for Electrochemical Supercapacitor. *Electrochimica Acta* **2006**, *52* (3), 1309–1315. https://doi.org/10.1016/j.electacta.2006.07.032.

View Article Online
DOI: 10.1039/D4YA00617H

(18) Ammar, A. U.; Yildirim, I. D.; Bakan, F.; Erdem, E. ZnO and MXenes as Electrode Materials for Supercapacitor Devices. *Beilstein J. Nanotechnol.* **2021**, *12* (1), 49–57. https://doi.org/10.3762/bjnano.12.4.

(19) Sasirekha, C.; Arumugam, S.; Muralidharan, G. Green Synthesis of ZnO/Carbon (ZnO/C) as an Electrode Material for Symmetric Supercapacitor Devices. *Appl. Surf. Sci.* **2018**, *449*, 521–527. https://doi.org/10.1016/j.apsusc.2018.01.172.

(20) Viswanathan, A.; Shetty, A. N. High Energy and Rate Capable Supercapacitor of Polyaniline / Vanadium Pentoxide Nanocomposite and Its Green Electrolyte. *Sustain.* **2025**, *5*, 100088. https://doi.org/10.1016/j.nxsust.2024.100088.

(21) Viswanathan, A.; Shetty, A. N. A Green Approach to Energy Storage Properties of Polyaniline. *Bull. Mater. Sci.* **2024**, *47* (4), 243. https://doi.org/10.1007/s12034-024-03329-7.

(22) Viswanathan, A.; Adka, N. S. Method and System for Synthesis of Electrode and Electrolyte Materials for High Energy Storage Devices. *Indian Pat. Off.* **2023**, *Application No. 201941044515* (Date of filing: 03/11/2019), Patent No. 450155.

(23) Ghorbani, H. R.; Mehr, F. P.; Pazoki, H.; Rahmani, B. M. Synthesis of ZnO Nanoparticles by Precipitation Method. *Orient J Chem* **2015**, *31* (2), 1219–1221.

(24) Madathil, A. N. P.; Vanaja, K. A.; Jayaraj, M. K. Synthesis of ZnO Nanoparticles by Hydrothermal Method. In *Nanophotonic Materials IV*; SPIE, 2007; Vol. 6639, pp 47–55. https://doi.org/10.1117/12.730364.

(25) Wang, F.; Qin, X.; Guo, Z.; Meng, Y.; Yang, L.; Ming, Y. Hydrothermal Synthesis of Dumbbell-Shaped ZnO Microstructures. *Ceram. Int.* **2013**, *39* (8), 8969–8973. https://doi.org/10.1016/j.ceramint.2013.04.096.

View Article Online
DOI: 10.1039/D4YA00617H

(26) Fang, Y.; Li, Z.; Xu, S.; Han, D.; Lu, D. Optical Properties and Photocatalytic Activities of Spherical ZnO and Flower-like ZnO Structures Synthesized by Facile Hydrothermal Method. *J. Alloys Compd.* **2013**, *575*, 359–363. https://doi.org/10.1016/j.jallcom.2013.05.183.

(27) Chandrasekaran, P.; Viruthagiri, G.; Srinivasan, N. The Effect of Various Capping Agents on the Surface Modifications of Sol–Gel Synthesised ZnO Nanoparticles. *J. Alloys Compd.* **2012**, *540*, 89–93. https://doi.org/10.1016/j.jallcom.2012.06.032.

(28) Lim, S. K.; Hwang, S.-H.; Kim, S.; Park, H. Preparation of ZnO Nanorods by Microemulsion Synthesis and Their Application as a CO Gas Sensor. *Sens. Actuators B Chem.* **2011**, *160* (1), 94–98. https://doi.org/10.1016/j.snb.2011.07.018.

(29) Wan, L.; Yan, S.; Feng, J.; Yang, Z.; Fan, X.; Li, Z.; Zou, Z. Solvothermal Synthesis of Core–Shell ZnO Hollow Microhemispheres. *Colloids Surf. Physicochem. Eng. Asp.* **2012**, *396*, 46–50. https://doi.org/10.1016/j.colsurfa.2011.12.039.

(30) Jiao, S.; Zhang, K.; Bai, S.; Li, H.; Gao, S.; Li, H.; Wang, J.; Yu, Q.; Guo, F.; Zhao, L. Controlled Morphology Evolution of ZnO Nanostructures in the Electrochemical Deposition: From the Point of View of Chloride Ions. *Electrochimica Acta* **2013**, *111*, 64–70. https://doi.org/10.1016/j.electacta.2013.08.050.

(31) Yue, S.; Lu, J.; Zhang, J. Controlled Growth of Well-Aligned Hierarchical ZnO Arrays by a Wet Chemical Method. *Mater. Lett.* **2009**, *63* (24), 2149–2152. https://doi.org/10.1016/j.matlet.2009.06.055.

(32) Ushio, M.; Sumiyoshi, Y. Synthesis of ZnO Single Crystals by the Flux Method. *J. Mater. Sci.* **1993**, *28* (1), 218–224. https://doi.org/10.1007/BF00349054.

(33) Wu, H.; Pan, W. Preparation of Zinc Oxide Nanofibers by Electrospinning. *J. Am. Ceram. Soc.* **2006**, *89* (2), 699–701. https://doi.org/10.1111/j.1551-2916.2005.00735.x.

View Article Online
DOI: 10.1039/D4YA00617H

(34) Hasanpoor, M.; Aliofkhazraei, M.; Delavari, H. Microwave-Assisted Synthesis of Zinc Oxide Nanoparticles. *Procedia Mater. Sci.* **2015**, *11*, 320–325. https://doi.org/10.1016/j.mspro.2015.11.101.

(35) Lee, S.; Jeong, S.; Kim, D.; Hwang, S.; Jeon, M.; Moon, J. ZnO Nanoparticles with Controlled Shapes and Sizes Prepared Using a Simple Polyol Synthesis. *Superlattices Microstruct.* **2008**, *43* (4), 330–339. https://doi.org/10.1016/j.spmi.2008.01.004.

(36) Ong, C. B.; Ng, L. Y.; Mohammad, A. W. A Review of ZnO Nanoparticles as Solar Photocatalysts: Synthesis, Mechanisms and Applications. *Renew. Sustain. Energy Rev.* **2018**, *81*, 536–551. https://doi.org/10.1016/j.rser.2017.08.020.

(37) Palsaniya, S.; Nemade, H. B.; Dasmahapatra, A. K. Hierarchical PANI-RGO-ZnO Ternary Nanocomposites for Symmetric Tandem Supercapacitor. *J. Phys. Chem. Solids* **2021**, *154*, 110081. https://doi.org/10.1016/j.jpcs.2021.110081.

(38) Pandiselvi, K.; Thambidurai, S. Chitosan-ZnO/Polyaniline Ternary Nanocomposite for High-Performance Supercapacitor. *Ionics* **2014**, *20* (4), 551–561. https://doi.org/10.1007/s11581-013-1020-0.

(39) Karthik, R.; Thambidurai, S. Synthesis of RGO–Co Doped ZnO/PANI Hybrid Composite for Supercapacitor Application. *J. Mater. Sci. Mater. Electron.* **2017**, *28* (13), 9836–9851. https://doi.org/10.1007/s10854-017-6738-4.

(40) Naveed ur Rehman, M.; Munawar, T.; Nadeem, M. S.; Mukhtar, F.; Akbar, U. A.; Manzoor, S.; Hakeem, A. S.; Ashiq, M. N.; Iqbal, F. Facile Synthesis of Novel PANI Covered Y2O3–ZnO Nanocomposite: A Promising Electrode Material for Supercapacitor. *Solid State Sci.* **2022**, *128*, 106883. https://doi.org/10.1016/j.solidstatesciences.2022.106883.

View Article Online
DOI: 10.1039/D4YA00617H

(41) Tonpe, D. A.; Gattu, K. P.; Kutwade, V. V.; Han, S.-H.; Sathe, B. R.; Sharma, R. ZnO-PANI Nanocomposite: Enhanced Electrochemical Performance towards Energy Storage. *J. Energy Storage* **2024**, *81*, 110434. https://doi.org/10.1016/j.est.2024.110434.

(42) Qin, D.; Zhou, B.; Li, Z.; Yang, C. Construction of Controllable Multicomponent ZnO-ZnCo/MOF-PANI Composites for Supercapacitor Applications. *J. Mol. Struct.* **2024**, *1309*, 138140. https://doi.org/10.1016/j.molstruc.2024.138140.

(43) Decremps, F.; Pellicer-Porres, J.; Saitta, A. M.; Chervin, J.-C.; Polian, A. High-Pressure Raman Spectroscopy Study of Wurtzite ZnO. *Phys. Rev. B* **2002**, *65* (9), 092101. https://doi.org/10.1103/PhysRevB.65.092101.

(44) Viswanathan, A.; Shetty, A. N. High Energy Supercapattery of Polyaniline/Cupric Oxide/Stannic Oxide Nanocomposite. *J. Phys. Chem. Solids* **2024**, *193*, 112141. https://doi.org/10.1016/j.jpcs.2024.112141.

(45) Jin, Y.; Jia, M. Design and Synthesis of Nanostructured Graphene-SnO2-Polyaniline Ternary Composite and Their Excellent Supercapacitor Performance. *Colloids Surf. Physicochem. Eng. Asp.* **2015**, *464*, 17–25. https://doi.org/10.1016/j.colsurfa.2014.09.032.

(46) Onyiriuka, E. C. Zinc Phosphate Glass Surfaces Studied by XPS. *J. Non-Cryst. Solids* **1993**, *163* (3), 268–273. https://doi.org/10.1016/0022-3093(93)91304-L.

(47) Haber, J.; Stoch, J.; Ungier, L. X-Ray Photoelectron Spectra of Oxygen in Oxides of Co, Ni, Fe and Zn. *J. Electron Spectrosc. Relat. Phenom.* **1976**, *9* (5), 459–467. https://doi.org/10.1016/0368-2048(76)80064-3.

(48) Gaarenstroom, S. W.; Winograd, N. Initial and Final State Effects in the ESCA Spectra of Cadmium and Silver Oxides. *J. Chem. Phys.* **1977**, *67* (8), 3500–3506. https://doi.org/10.1063/1.435347.

View Article Online
DOI: 10.1039/D4YA00617H

(49) Chastain, J.; King Jr, R. C. Handbook of X-Ray Photoelectron Spectroscopy. *Perkin-Elmer Corp.* **1992**, *40*, 221.

(50) Di Giulio, M.; Micocci, G.; Serra, A.; Tepore, A.; Rella, R.; Siciliano, P. SnO2 Thin Films for Gas Sensor Prepared by r.f. Reactive Sputtering. *Sens. Actuators B Chem.* **1995**, *25* (1), 465–468. https://doi.org/10.1016/0925-4005(94)01397-7.

(51) Choi, W.; Jung, H.; Koh, S. Chemical Shifts and Optical Properties of Tin Oxide Films Grown by a Reactive Ion Assisted Deposition. *J. Vac. Sci. Technol. A* **1996**, *14* (2), 359–366. https://doi.org/10.1116/1.579901.

(52) Fan, J. C. C.; Goodenough, J. B. X-ray Photoemission Spectroscopy Studies of Sn-doped Indium-oxide Films. *J. Appl. Phys.* **1977**, *48* (8), 3524–3531. https://doi.org/10.1063/1.324149.

(53) Viswanathan, A.; Shetty, A. N. The High Energy Yielding Supercapattery of PANI/VO2 Binary Nanocomposite. *Future Batter.* **2024**, *4*, 100009. https://doi.org/10.1016/j.fub.2024.100009.

(54) Viswanathan, A.; Acharya, M. G.; Prakashaiaha, B. G.; Shetty, A. N. Superior Supercapacitance Exhibited by Acid Insoluble Ni(OH)2 in the Form of Its Nanocomposite with rGO. *J. Energy Storage* **2022**, *55*, 105527. https://doi.org/10.1016/j.est.2022.105527.

(55) Viswanathan, A.; Shetty, A. N. High Energy Supercapacitance of Magnetic PANI/Ni2O3 Nanocomposite and Its Magnetic Structural Repair. *J. Energy Storage* **2024**, *90*, 111759. https://doi.org/10.1016/j.est.2024.111759.

(56) Viswanathan, A.; Shetty, A. N. Effect of Dopants on the Energy Storage Performance of Reduced Graphene Oxide/Polyaniline Nanocomposite. *Electrochimica Acta* **2019**, *327*, 135026. https://doi.org/10.1016/j.electacta.2019.135026.

View Article Online
DOI: 10.1039/D4YA00617H

(57) Dunn, B.; Dunn, B.; Kamath, H.; Tarascon, J. Electrical Energy Storage for the Gridfor the Grid : A Battery of Choices. *Sci. Mag.* **2011**, *334* (6058), 928–936. https://doi.org/10.1126/science.1212741.

(58) Siva, T.; Kamaraj, K.; Sathiyanarayanan, S. Epoxy Curing by Polyaniline (PANI) – Characterization and Self-Healing Evaluation. *Prog. Org. Coat.* **2014**, *77* (6), 1095–1103. https://doi.org/10.1016/j.porgcoat.2014.03.019.

(59) Adnan, S. M.; Shoeb, M.; Ansari, M. Z.; Mashkoor, F.; Mobin, M.; Zaidi, S.; Jeong, C. Fabrication of NiO–CuO Decorated Polyaniline (PANI/NiO–CuO) Nanocomposite Based Symmetric Supercapacitor Device for High-Energy Density Performance with Wide Potential Window in Aqueous Electrolyte. *Inorg. Chem. Commun.* **2023**, *157*, 111265. https://doi.org/10.1016/j.inoche.2023.111265.

(60) Naveed ur Rehman, M.; Munawar, T.; Nadeem, M. S.; Mukhtar, F.; Akbar, U. A.; Manzoor, S.; Hakeem, A. S.; Ashiq, M. N.; Iqbal, F. Facile Synthesis of Novel PANI Covered Y2O3–ZnO Nanocomposite: A Promising Electrode Material for Supercapacitor. *Solid State Sci.* **2022**, *128*, 106883. https://doi.org/10.1016/j.solidstatesciences.2022.106883.

(61) Purty, B.; Choudhary, R. B.; Kandulna, R.; Singh, R. Remarkable Enhancement in Electrochemical Capacitance Value of Ag-ZnO/PANI Composite for Supercapacitor Application. *AIP Conf. Proc.* **2019**, *2115* (1), 030588. https://doi.org/10.1063/1.5113427.

View Article Online
DOI: 10.1039/D4YA00617H

Data availability statement

The data generated during and/or analysed during the current study are available from the corresponding author on reasonable request